3.0. IDENTIFICATION OF RESEARCH AREA FOR FIELD STUDY

Coal mining began in JCF in the early 1890's more than 100 years ago and is still continuing. The crescent shaped basin of the coalfield had 1 billion tonnes of proven coal reserves. BCCL is the primary mining agency in this area and it supplies about 50% of the nation's coking coal to steel sector (http://www.bcclweb.in/).

In India, large sized CSF are located in Jharia, Raniganj, Singrauli and Singareni coalfields. Of these, Jharia CSF are continuing for the longest time period and are most harmful and extensive in terms of area.

The area selected for the study had complex coal fire. Thus, it had become unviable for the JCF. The study site was bounded with 23 ° 38 ' N and 23 ° 50' N latitudes and 86 ° 07 'E and 86 ° 30' E longitudes. The JCF spreads approximately 40 km east- west and 12 km north-south with a total area of 480 km^2. The town of Jharia is located at the north of Damodar River.

The coalfield has more than 40 operating coal mines. Mining here was adopting both open cast and underground method but majority of the mines was open cast. The population over the affected areas and over the underground mining areas was 1.1 million. The topography is gently undulating to rolling with a slope towards east southeast. The JCF belongs to Gondwana Permian age group with Talchir, Barakar, Barren Measures and Raniganj Formations. The geological coal reserves of JCF within the lease hold of Bharat Coking Coal Limited (BCCL) are up to a depth of 200m.

Presently, handling JCF for mining and reducing its impact on its stakeholders is getting more difficult. JCF had several thick coal seams located at shallow depths. Further, it has faced

huge land degradation, severe mine fires and rampant environmental pollution. It is considered to be one of the world's most degraded coalfields. Land subsidence is also one of the major land degradation aspects of this coalfield. Therefore,

its scientific planning is constrained due to problems of the fires, buildings, and other existing important surface structures.

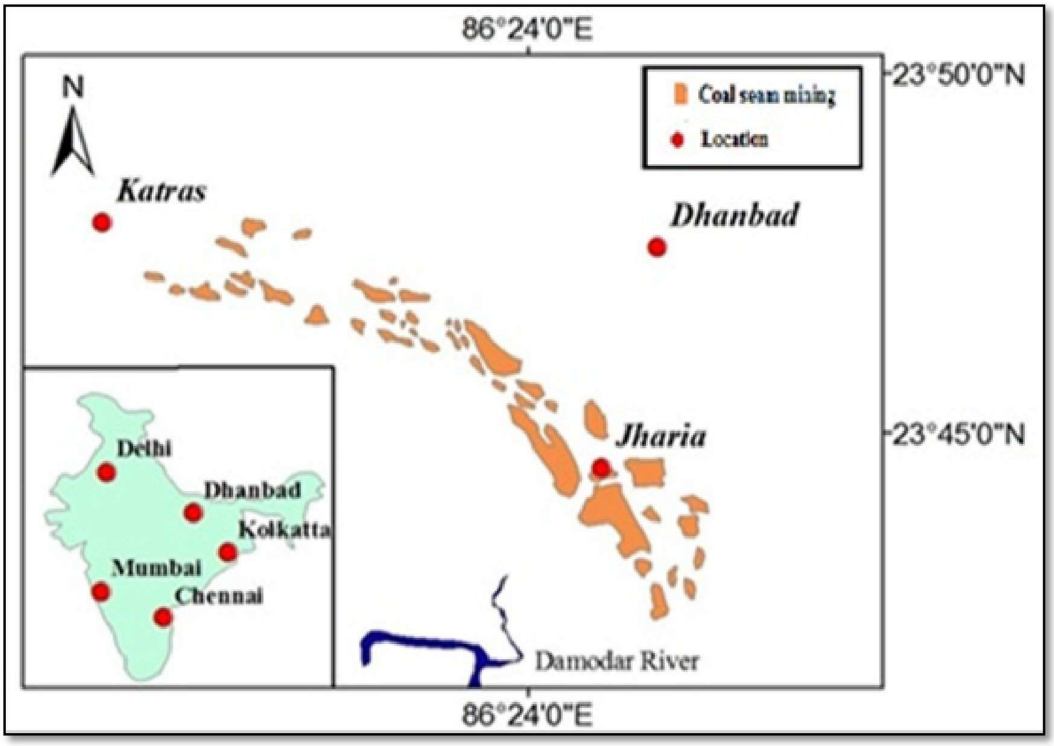

Fig: 7 Location Map of JCF

The photographs taken during the field investigations depict the level of CSF and are given below:

Fig: 8 Live and open CSF from fire chamber at Katrasgarh

The Fig. 8 shows that the fire is live and surfacing out from the weak zones and burning with the internal fuels of the underground coal seam.

`

Fig: 9 Open CSF visible at the weak zones

`

Fig: 10 Surface subsidence due to Kusunda CSF

The subsidence in the JCF is caused due to the formation of the cavity due to the burning of the coal of the under lying supporting coal layers.

`

Fig: 11 Visible and severe Cracks on houses due to subsidence in Jharia area

The foundation of the building structures are losing support due to sub surface subsidence resulting from the cavities caused due to burning of the coal seams below them due to their consumption through coal fire. When the nature of the stress changes from the compressive to tensile, the foundations and the walls of the buildings and structures face this kind of vertical fractures.

Fig: 12 CSF on working benches in Katrasgarh Mines

`

Fig: 13The worker near the CSF on the abandoned & daylighted shaft

Fig: 14 Visible CSF at the fissures depicting the development of fire chamber

The CSF is visible in the weak zones at the fissures & cracks.

`

Fig: 15 Blue flame due to methane in CSF at the night time

`

3.2 EXISTING GEO-MINING CONDITIONS IN JCF

The geo-mining conditions like surface topography, soil, geographical, geological, hydro geological conditions and the method of mining are influencing the CSF formation and propagation in the JCF. Hence, its existing realities are chronicled here.

3.2.1 Physiography

The Parasnath hills and the associated thick forest abound the northern part of the study area. The lowest observed altitude was 132m msl at Chirkund and highest was 747m msl at Parasnath. Geologically, the region falls within the Barakar region which is in the vicinity of the Damodar River and its tributaries. This area consists of coalfields and landfills.

The main geomorphic features and landforms (illustrated in Fig 18) of the district are as follows.

3.2.1.1 Alluvial Plain:- They are located near the river valleys and have gravel, sand, bridge, clay, etc.

3.2.1.2 Structural Ridge: - The linear or curved hills that looks trendy and covered with thick forests evolve against metamorphic rocks. They are found in Tundi and in the northern part of the Topchanchi region.

3.2.1.3 Pediplains over meta sediment:- These are developed with granite-gneiss and meta sediment. These are found in the Govindpuri block and in the Tundi block

3.2.1.4 **P**ediplain over sedimentary:- Gondwana formation. These are located in Nirsa area.

3.2.1.5 Dissected Pediplain:- Dissected pediplains are in Gondwana formations and are found in Katras area.

3.2.1.6 Denudation hill: - These hills are enveloped over metamorphic rocks and located as moderately high hills and are mostly barren rocky exposure, located in north eastern/Northwestern parts of the district.

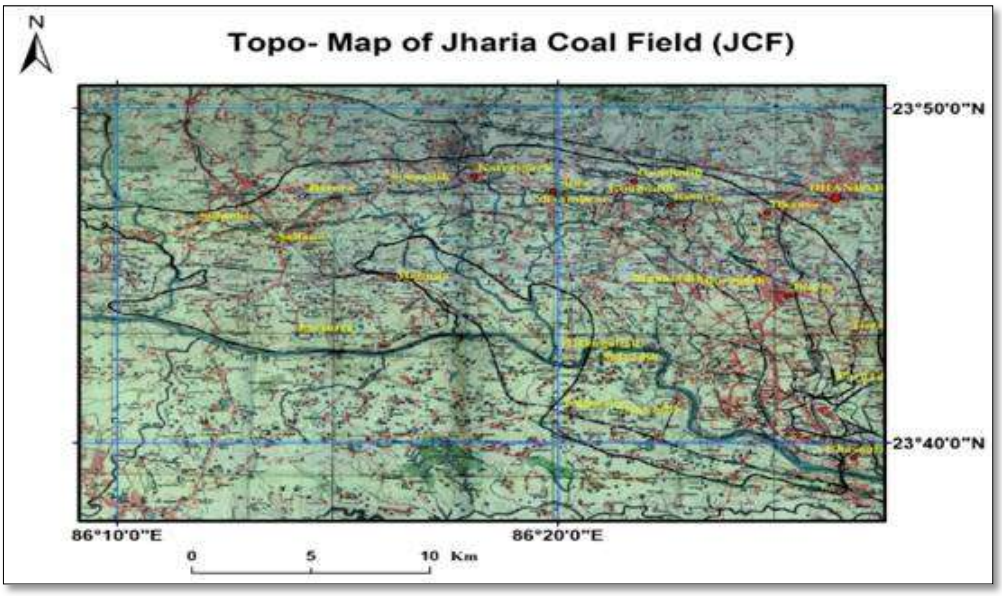

Fig: 16 The JCF is marked on the toposheet of Survey of India through Arc Map software.

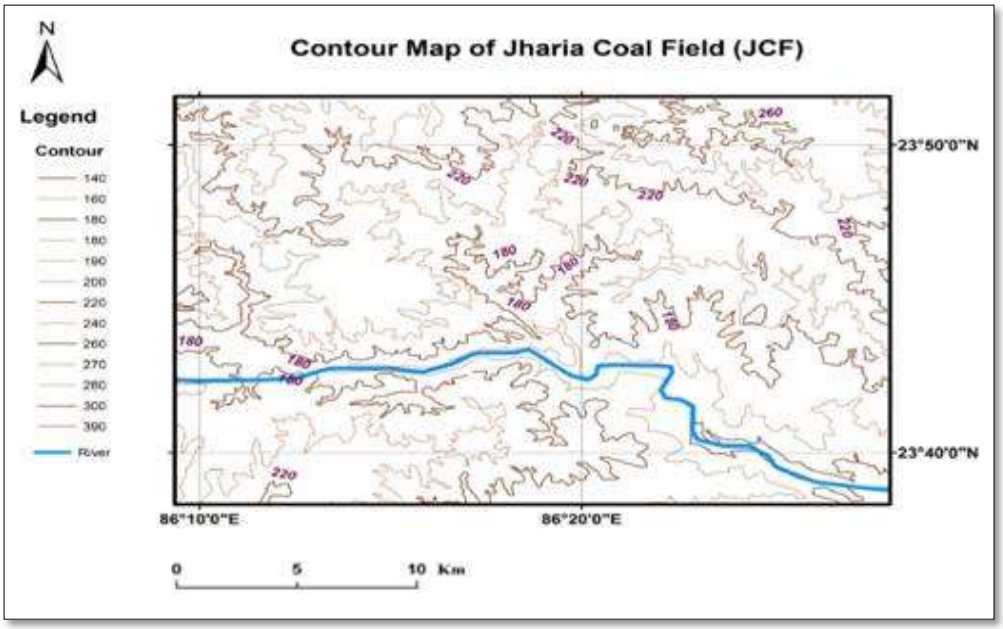

Fig: 17 Contour Map of JCF

`

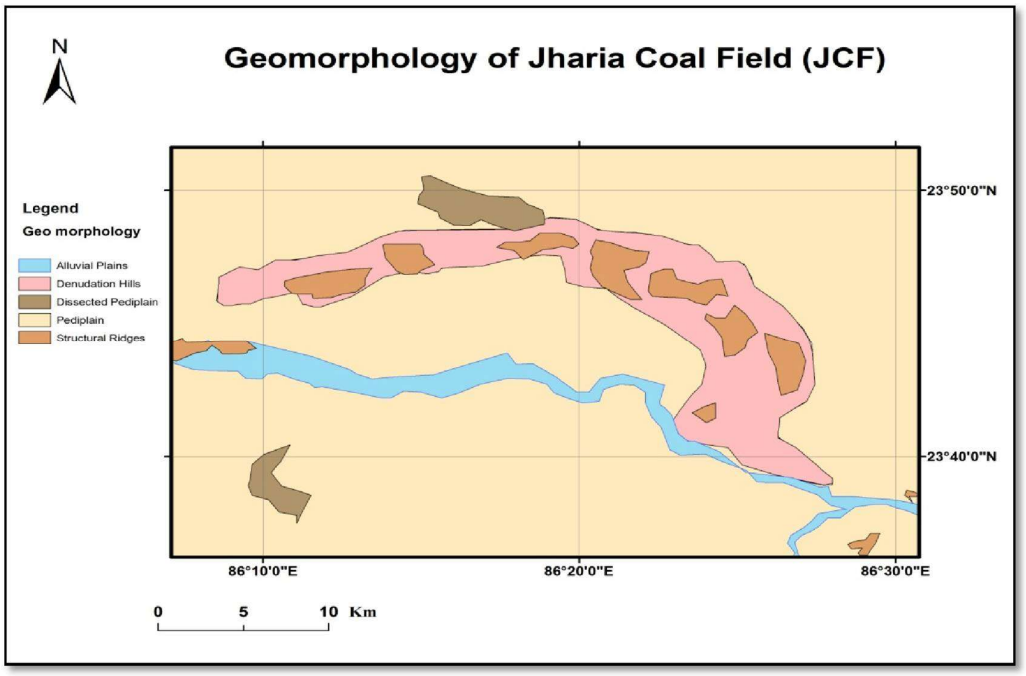

Fig: 18 Geomorphology Map of JCF

3.2.2 SOIL OF THE JCF

The soil is mostly residual product. High temperatures and rock which is exposed in most of the field and also at the lower Gondwana rock in the western and central parts. The soil in the area is classified into four categories.

3.2.2.1 a. Stony and Gravel Soil: - These are low-grade soils having a large admixture of cobbles, pebbles and gravels generally found at the base of the hills.

b. Sandy soils— these types of soils are generally found near the river and streambeds. They contain more than 60 percent sand and are poor in plant nutrients. They are also called hungry soils because of heavy managing required.

3.2.2.2 Loamy Soil: comprise mostly of the detritus of the decomposed rocks and vegetable matters that are found to be in the range of 30 to 60 per cent.

3.2.2.3 Clayey Soil: These soils are sticky when wet and very hard when dry.

3.2.3 HYDROGEOLOGY OF JCF

The groundwater conditions affect the CSF of JCF. The ground water is present under confined zones at shallow depths in most of the Achaean litho units and almost all Gondwana units. Groundwater occurs only in a partially restricted state at the fractures.

Shallow Aquifers: - The shallow aquifers are being tapped through dug wells, dug cum bore wells or shallow bore wells drilled up to the depth of 60 m.

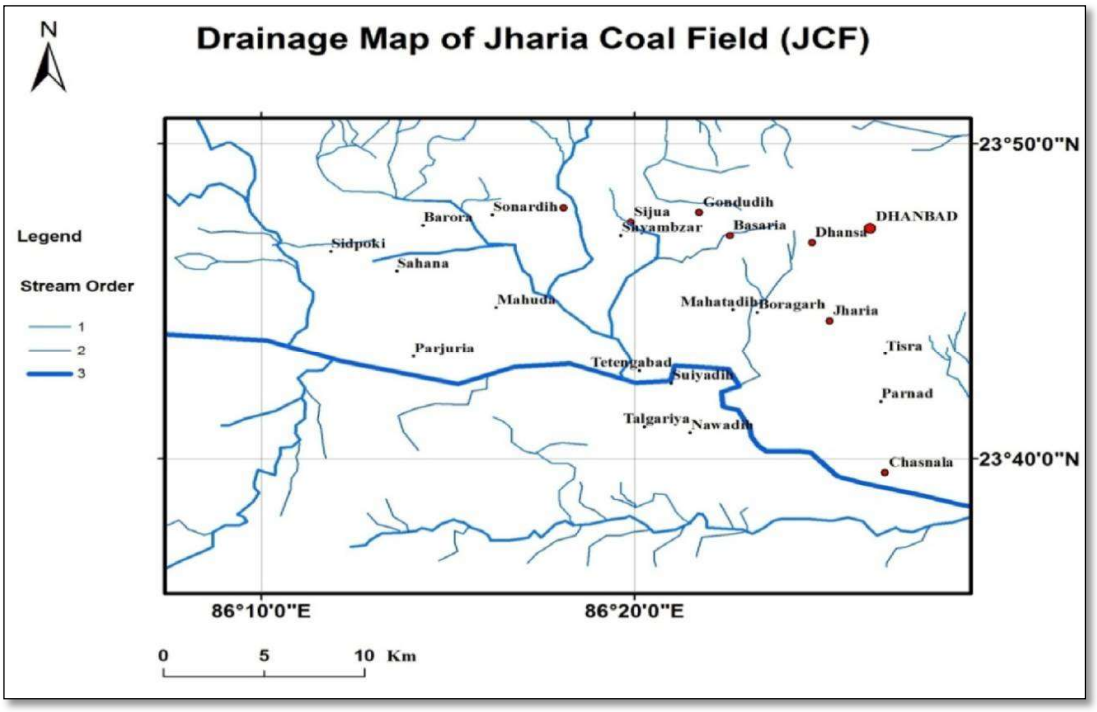

Fig: 19 Drainage Map of JCF

3.2.4 GEOLOGY OF THE JCF

Geology includes the number, thickness and continuity of the geological structure, the number of coal seams, and the extent and the location of the mica-peridotite intrusive. It also reports faults, dykes and coal seam outcrops.

It plays dominant role in the exploration, in estimating the thickness of the coal seam and the location, coal seam behaviour, in situ coal quality, coal marketability and the proneness of the coal seam to fire. The probable location of the CSF has immense potential to impact mine planning and operations.

Geological succession in the JCF is detailed in the Table no 5 given below.

Table: 5 Geological succession of JCF

Age	Litho- unit	Rock Type/Name
Recent		River Alluvium
Jurassic or Tertiary	Rajmahal or Deccan Trap	Dolerite Dyke
Lower Jurassic	Rajmahal or earlier	Mica Lamprophyre Dykes and Sills
Upper Permian	Raniganj Formation (570m)	Lohpiti (Sandstones) & Kangra Stage
		Telmucha Stage (with coal seams)
		Jamdiha Stage (Sandstones)
		Murulidih Stage(with coal seams)
Middle Permian	Barren Measures (615m)	Mahuda Stage(Sandstones, 182.87m)
		Hariharpuri Stage(with coal seams)
		Petia Stage (Sandstones, 182.87m)
		Bhelatand Stage(Shibudih Shales)
Lower Permian	Barakar Formation (620m)	4Bhagaband Stage(seams XVI-XVII) (Darari Stage with seams of Gararia & Tisra)
		3 Jealgora Stage (seams XVI- XVII)
		2. Nardkarki Stage(seams I- VII) (Golakdih Stage with seams of Muraidih &
		1.Muraidih Stage (seam I-VII)
Upper Carboniferous	Talchir Formation	Green Shales with nodular and needle shaped weathering, fine khaki- colored sandstone boulder bed
----------Unconformity ----------		
	Archeans	Crystalline rock

Sharma [114]& GSI[115]

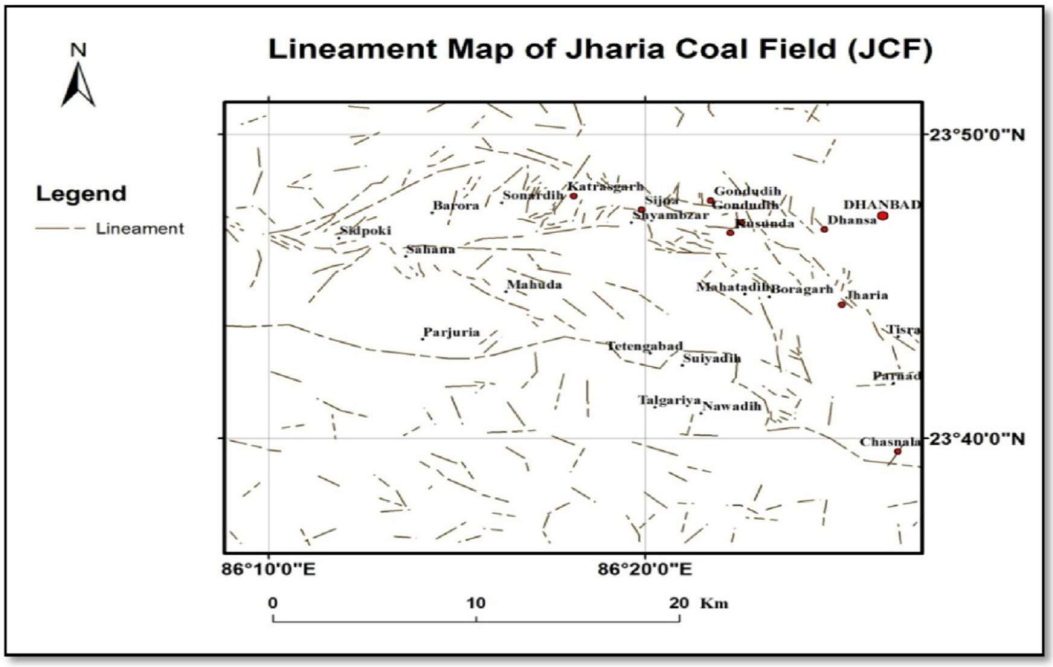

Fig: 20 Lineaments obtained from satellite image of JCF

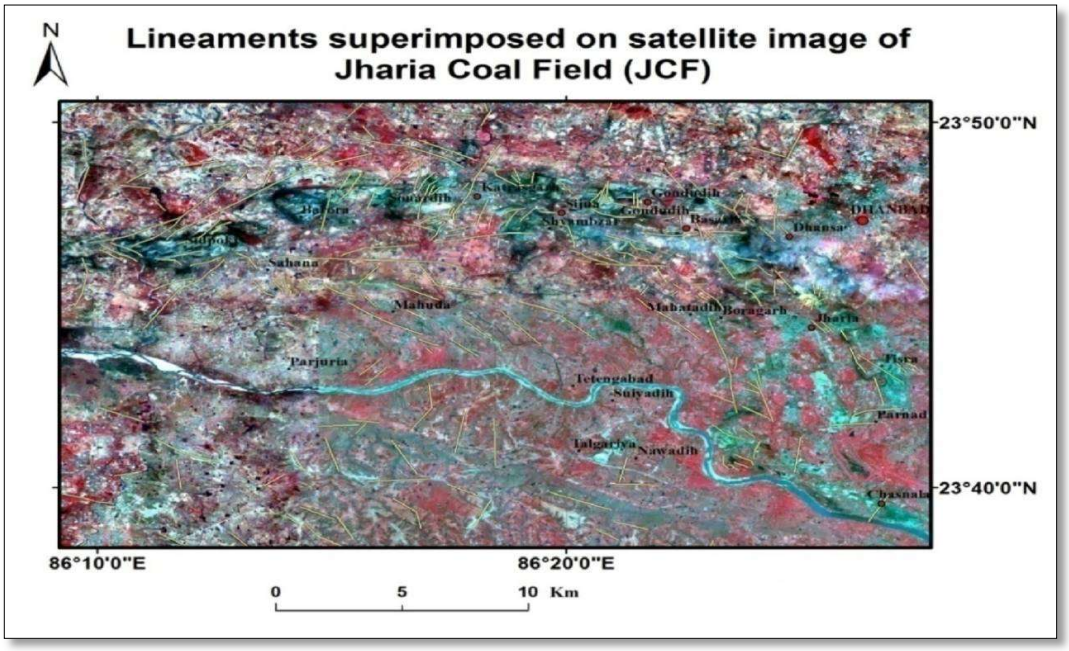

Fig: 21 Lineaments superimposed on satellite image of JCF

The maximum lineaments are trending in NNW, SEW and NS as depicted in figure 20.

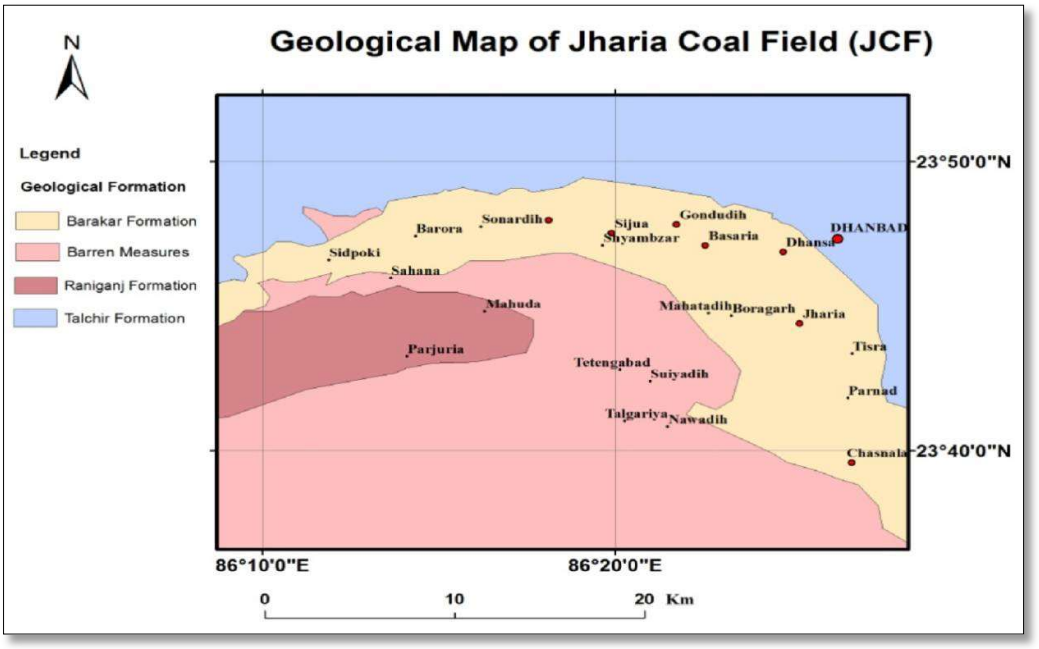

Fig: 22 Geological Map of JCF

Table: 6 Methods deployed for the analysis of the CSF of JCF

Methods Deployed	Techniques	Satellite Data
Major Tool RS and GIS with ERDAS and Arc Map	Band Ratioing	1972, 1980, 2007, 2008, 2009, 2011, 2012 and 2013
	Histogram Equalizations	
Principal Component Analysis (PCA)	Functions	
Classification	Un - Supervised	
	Supervised	
Field Validation	CSF Field Mapping	Toposheets, SRTM DEM, Google Image, BCCL Fire Map
Geo Tagging	Mapping	SRTM DEM

SATELLITE IMAGE ANALYSIS

3.3. NORMALISED DIFFERENCE VEGETATION INDEX

3.3.1 DYNAMICS OF WATER CONTENTS

As discussed earlier, CSF adversely affects the land surface and subsurface along with its nutrients and therefore severely damages the vegetation of the area within the influence zones. Thus, the study of the growth of vegetation and its existing profile and temporal degradation, obtained through the satellite data, can be effectively utilized for demarcating the area under CSF. Therefore, the vegetation had been analyzed with RS data by using vegetation index. The vegetation index correlates with the chlorophyll content of plants. The high values of vegetation marks are covered by substantial proportions of strong vegetation. NDVI is important in the activity of photography and it has been found that it is associated with the green area index which is the result of the active radiation that the vegetation has taken. The NDVI provides the impact of fire over the vegetation of the area under study.

3.3.2 NDVI MODEL OF DIGITAL VALUE SIMULATIONS

The CSF movement over existing vegetation's of the area can be effectively evaluated using satellite data. The vegetation were analyzed through RS by using indexes. The high values of the NDVI depicts active vegetation index and conveys that the area is covered by substantial proportions of strong vegetation. NDVI has been found that it is associated with the green area, which is the result of the indices obtained.

Fig 23 shows the NDVI image of JCF in 1972 where the index can be seen to range from - 0.552 to 0.555. Then, the lowest values of NDVI were shown in red color and the highest in color green.

It can be noted that the density of the vegetation was lower in the northern part of the area and higher on the mineral bearing areas.

Fig 24 shows the NDVI image of JCF in 1980. Here, the index was in the range from 0.664 to 0.569. The lowest values of NDVI were shown in red color and the highest color in green.

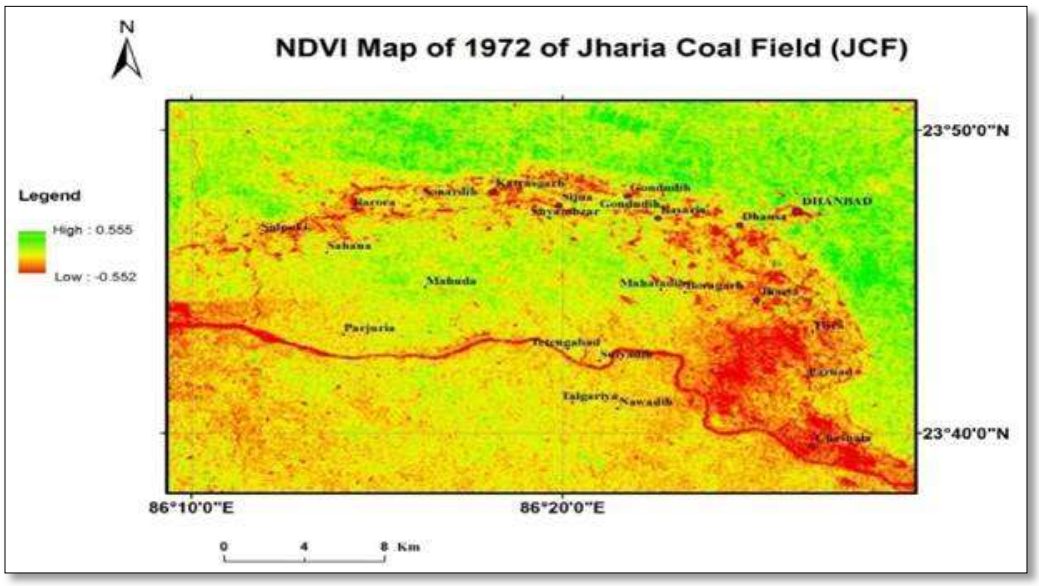

Fig: 23 NDVI Map of 1972 of JCF

The Fig 23 depicts the NDVI image of JCF in 1972 and it may be observed that the index varied as obtained through ERDAS imagine. Here, the lowest values of NDVI were shown in red colour and the highest in green colour. It may be observed that the vegetation density was lower in the northern side of the area and higher on mineral bearing sites.

The Fig 24 shows the NDVI image of JCF in 1980. Here, it may be observed that the index varied from - 0.664 to0.569, as obtained through ERDAS imagine. The lowest values of NDVI were shown in red colour and the highest in green colour. It may be observed that the vegetation density was lower in northern side of the area and higher on mining sites.

The Fig : 25 depicts the NDVI image of JCF in 2007, here, it may be observed that the index varied from – 0.550 to 0.553, as obtained through ERDAS imagine. The lowest values of NDVI were shown in red colour and the highest in green colour. It may be observed that the vegetation density is lower in northern side of the area and higher on mining sites.

The Fig : 26 depicts the NDVI image of JCF in 2008 where it was found that the index varied from – 0.559 to 0.661, as obtained through ERDAS imagine. The lowest values of NDVI were shown in red colour and the highest in green colour. It may be observed that the vegetation density is lower in northern side of the area and high on mining sites.

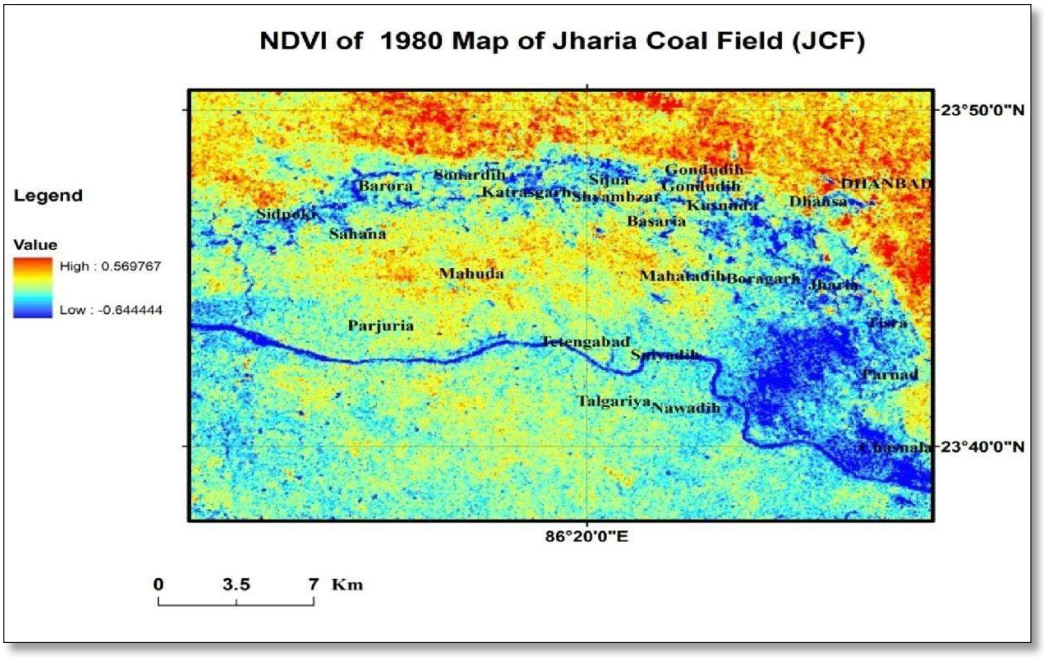

Fig: 24 NDVI Maps of 1980 of JCF

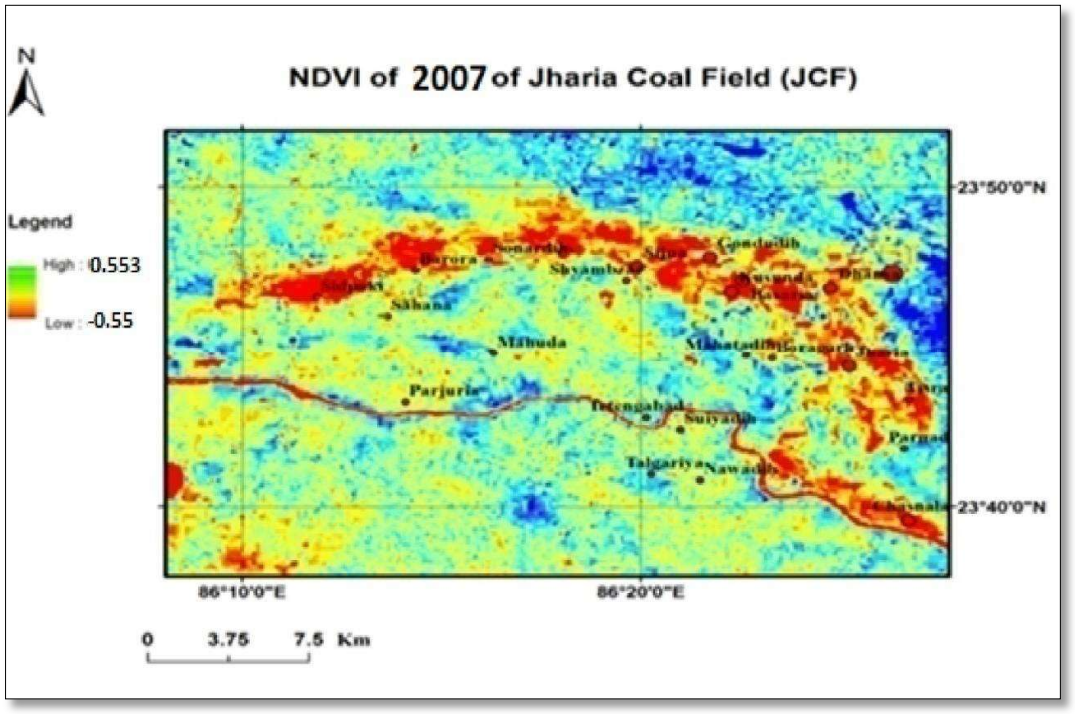

Fig: 25 NDVI Maps of 2007 of JCF

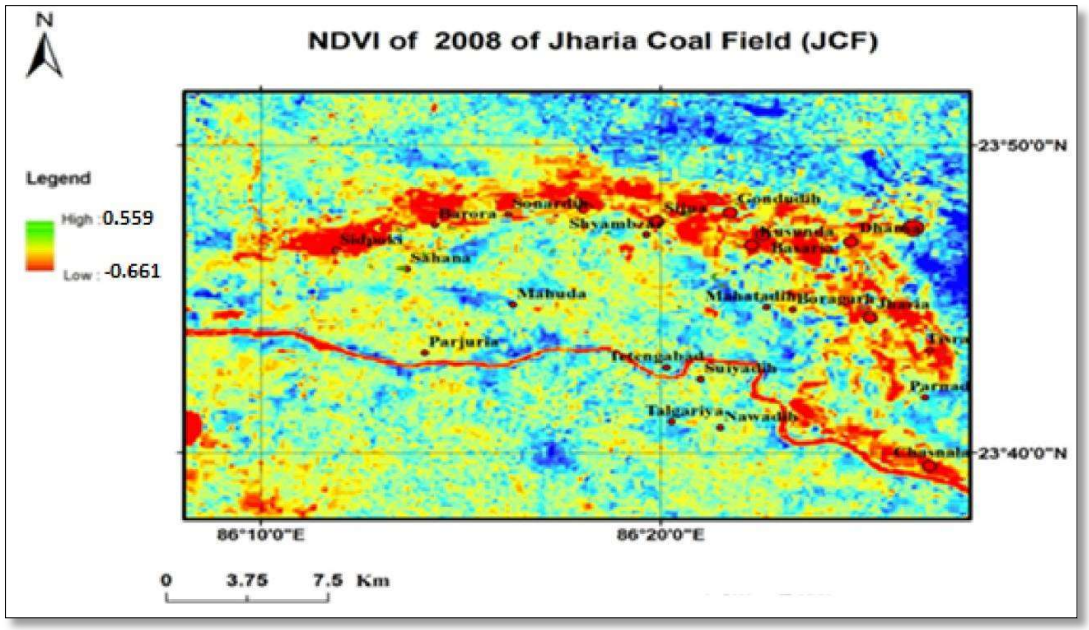

Fig: 26 NDVI Map of 2008 of JCF

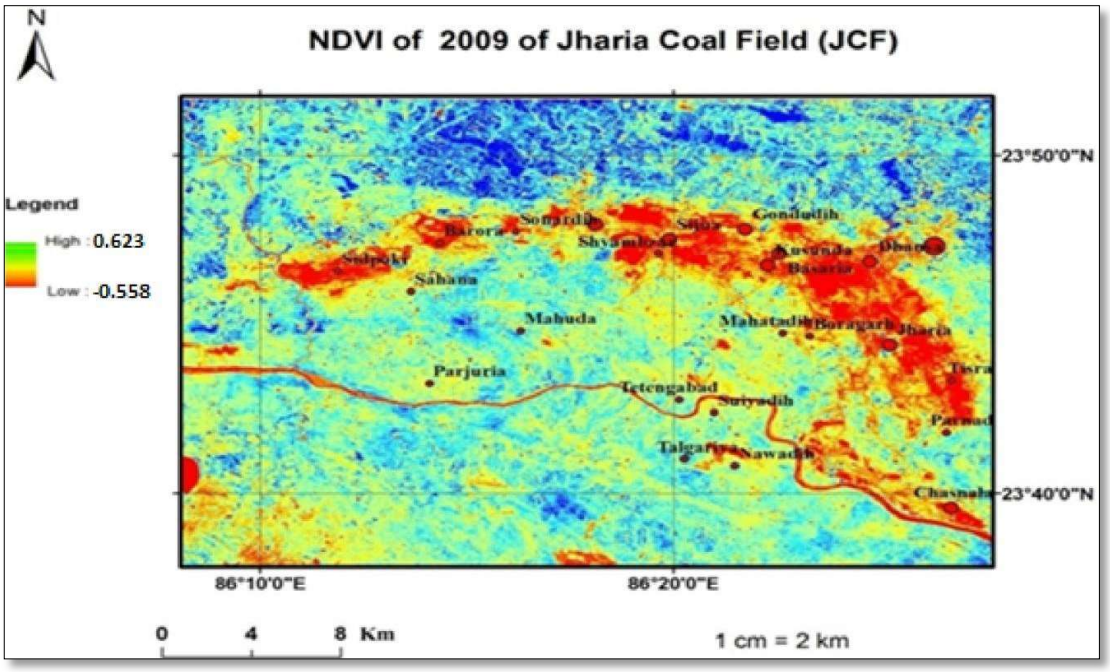

Fig: 27 NDVI Maps of 2009 of JCF

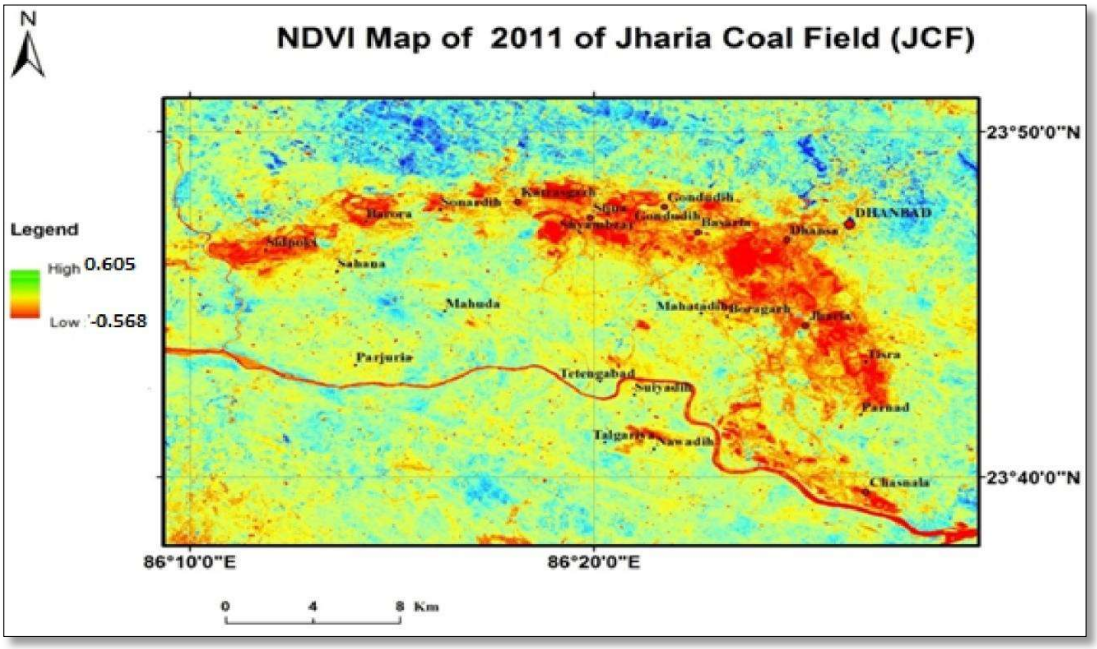

Fig: 28 NDVI Maps of 2011 of JCF

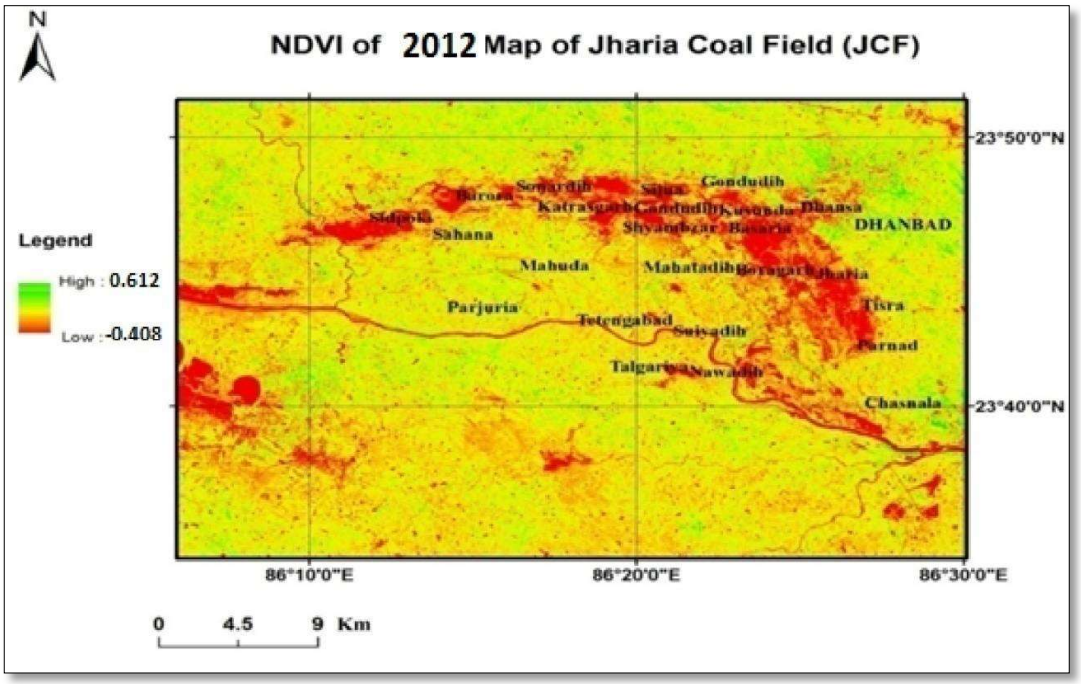

Fig: 29 NDVI Maps of 2012 of JCF

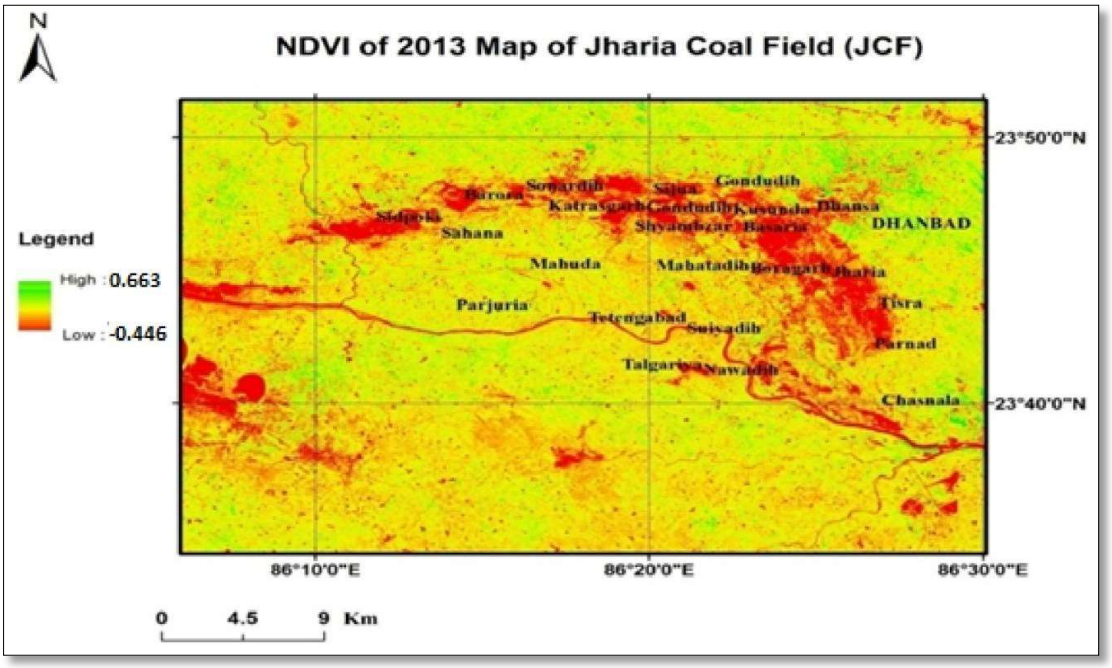

Fig: 30 NDVI Map of 2013 of JCF

The Fig: 27 depicts the NDVI image of JCF in 2009 wherein it was observed that the index varied from – 0.558 to 0.623, as obtained through ERDAS imagine. The lowest values of NDVI were

shown in red colour and the highest in green colour. It may be observed that the vegetation density is lower in northern side of the area and high on mining sites.

The Fig : 28 depicts the NDVI image of JCF in 2011 wherein it may be observed that the index varied from – 0.568 to 0.605, as obtained through ERDAS imagine. The lowest value of NDVI was shown in red colour and the highest in green colour. It may be observed that the vegetation density is lower in north eastern and south eastern part of the area and high on mining sites.

The Fig: 29 shows the NDVI image of JCF in 2012 wherein it may be observed that the index varied from – 0.408 to 0.612, as obtained through ERDAS imagine. The lowest values of the NDVI was shown in red colour and the highest in green colour. It may be observed that the vegetation density is lower in northern side of the area and partially higher on the mining sites.

The Fig: 30 depicts the NDVI image of JCF in 2013 wherein it may be observed that the index varied from – 0.446 to 0.663, as obtained through ERDAS imagine. The lowest values of NDVI were shown in red colour and the highest in green colour. It may be observed that the zone with the higher NDVI is shrinking. It implies that the vegetation density is lower in northern side of the area and NDVI is lower for larger portion of the mining sites.

The summaries of NDVI inferences drawn from the imageries of the different time periods for the JCF are given below in the Table no.6. The table depicts that the maximum vegetation was in 2008 and minimum vegetation was observed in 2013. A trend was observed that the distribution of the vegetation on the northern side of JCF was always lower than that of the southern side of the JCF, within the same year and at any given time.

Table: 7 Inference drawn from NDVI Analysis

S. No.	Figure No.	Year	Maxima	Minima	Inference
1	23	1972	0.555	-0.552	The vegetation are lower in northern side
2	24	1980	0.569	-0.644	The vegetation are lower in north-eastern side
3	25	2007	0.553	-0.55	The vegetation are lower in north-eastern side and lower in south eastern
4	26	2008	0.559	-0.661	The vegetation are lower in north-eastern side
5	27	2009	0.623	-0.558	The vegetation are lower in northern side
6	28	2011	0.605	-0.568	The vegetation are lower in north-eastern side
7	29	2012	0.612	-0.408	The vegetation are lower in the whole area, southern side and mining sites
8	30	2013	0.663	-0.446	The vegetation are lower in JCF area

When the value approaches 1 , it is an indicator of the healthy vegetation (green content) 0.29 or less area of barren rock, sand and 0.30 to 0.70 for shrubs and grassland , 0.71 to 1.0 is for dense vegetation .

prediction of surface temperatures in JCF.

In the year 1972 maxima 0.555 and minima is – 0.552. The visual analysis of image by indices of sub pixel and grid predicts the surface temperature with the density of vegetation. The vegetation are lower in northern side

In the year 1980 maxima 0.569 and minima of – 0.644. The visual analysis of image by indices of sub pixel and grid predicts the surface temperature with the density of vegetation. The vegetation are lower in north-eastern side. The pixels in the kernel of grid considered as the single unit and

In the year 2007 maxima 0.553 and minima of – 0.55. The visual analysis of image by indices of sub pixel and grid predicts the surface temperature with the density of vegetation. The vegetation are lower in north-eastern side and lower in south eastern

In the year 2008 maxima 0.559 and minima is – 0.661. The visual analysis of image by sub pixel and grid by indices predicts surface temperature with the density of vegetation. The vegetation are lower in north-eastern side

In the year 2009 maxima 0.623 and minima of – 0.558. The visual analysis of image by indices of sub pixel and grid predicts the surface temperature with the density of vegetation. The vegetation are lower in northern side

In the year 2011 maxima 0.605 and minima of – 0.568. The visual analysis of image by indices of sub pixel and grid predicts the surface temperature with the density of vegetation. The vegetation are lower in north-eastern side.

In the year 2012 maxima 0.612 and minima of – 0.408. The visual analysis of image by indices of sub pixel and grid predicts the surface temperature with the density of vegetation. The vegetation are lower in the whole area, southern side and mining sites

In the year 2013 maxima 0.663 and minima of – 0.446. The visual analysis of image by indices of sub pixel and grid predicts the surface temperature with the density of vegetation. The vegetation are lower in JCF area.

3.4 CUMULATIVE DISTRIBUTION FUNCTION

This method increases the contrast of images whenever the images are represented by close contrast values. These adjustments are based on the intensities distributed on the histogram. This allows for the areas of lower local contrast to gain a higher contrast. Histogram equalization accomplishes this by effectively spreading out the most frequent intensity values.

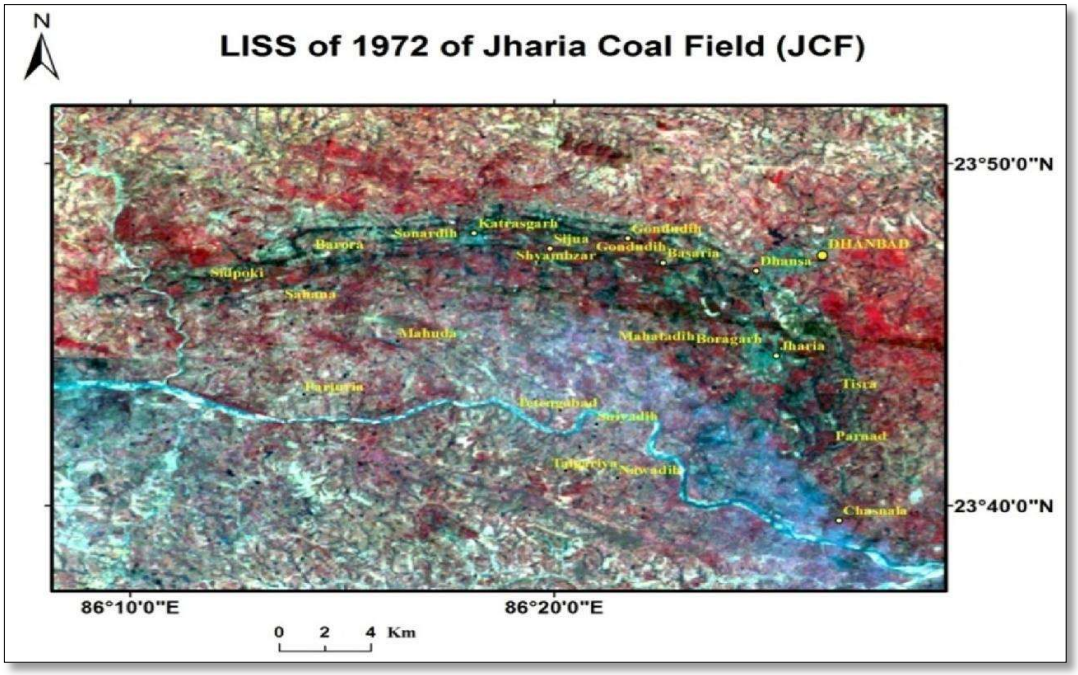

Fig: 31 LISS image of 1972 of JCF

The various bands of satellite image shows vegetation and CSF in different tones. The Histogram Equalization shows the segmentation of pixel values for better interpretations. The low vegetation cover shows peak and high vegetation cover shows non-peak regions.

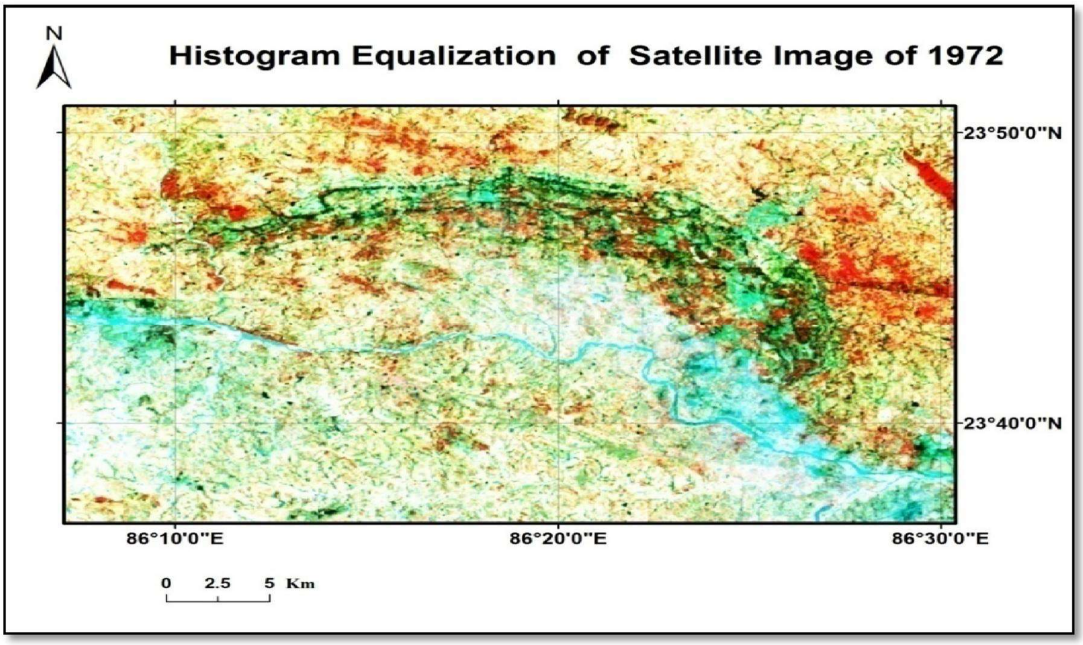

Fig: 32 Histogram Equalization image of 1972 of JCF

The segmentation of pixel values shows the lowest reflectance 0.00 to max reflectance of 218 as digital numbers of pixels. And their standard deviation is 12.51 in red band of image. It depicts that the vegetation and other classes were mixed in the red bands.

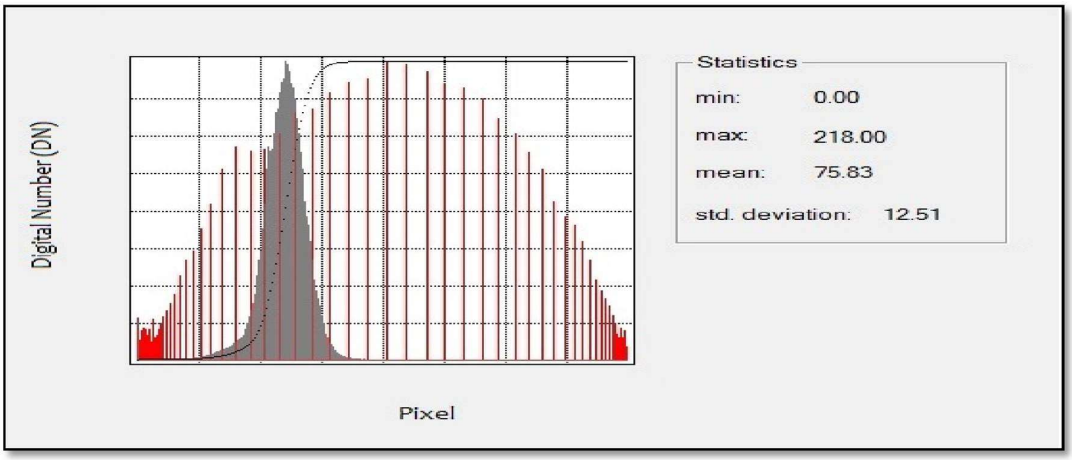

Fig: 33 Histogram Equalization statistics of image in Red Band of 1972 of JCF

The segmentation of pixel values shows the lowest reflectance 0.00 to max reflectance of 195 as digital numbers of pixels. Their standard deviations are 51.38 in green band of image. It depicts that the vegetation and other classes of medium value reflectance were mixed in the green bands.

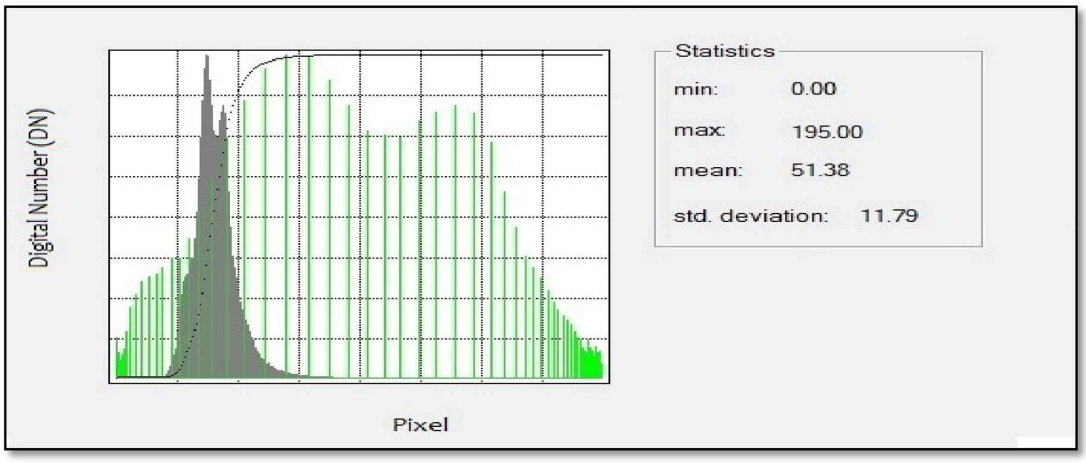

Fig: 34 Histogram Equalization of image in Green Band of 1972 of JCF.

The segmentation of the pixel values depict the lowest reflectance 0.00 to max reflectance of 245 as digital numbers of pixels. Their standard deviations were 8.5 in blue band of image. It shows that the vegetation and other classes were mixed in the red bands.

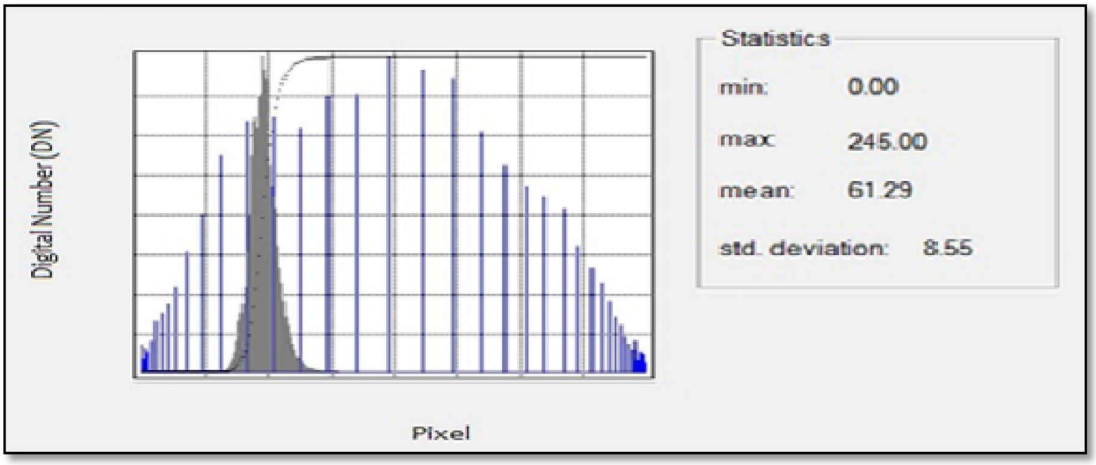

Fig: 35 Histogram Equalization statistics of image in Blue Band of 1972 of JCF

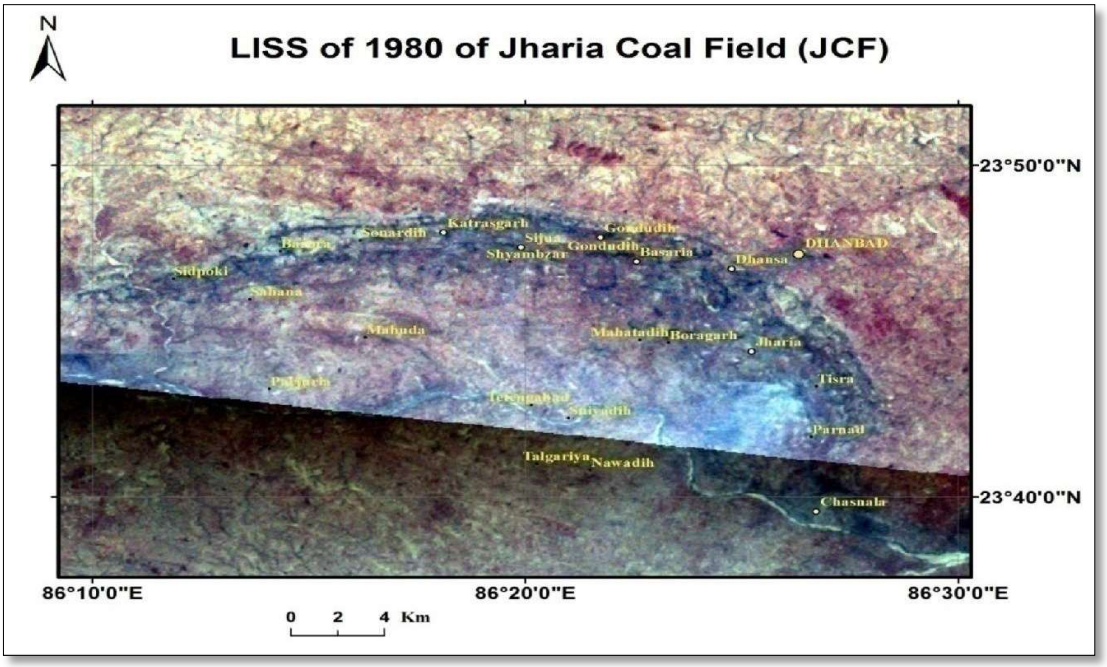

Fig: 36 LISS image of 1980 of JCF

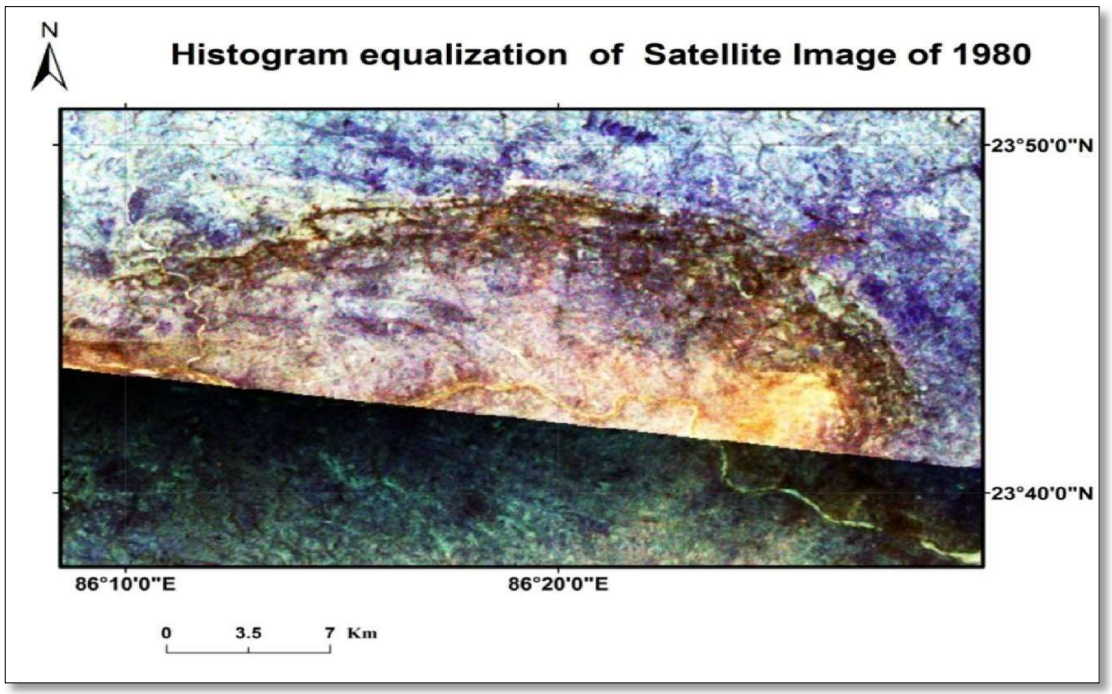

Fig: 37 Histogram Equalization images of 1980 of JCF

The segmentation of pixel values shows the lowest reflectance 0.00 to max reflectance of 98 as digital numbers of pixels. Their standard deviations are 41.22 in red band of image. It depicts that the chances of mixing of vegetation and other classes in this band is more.

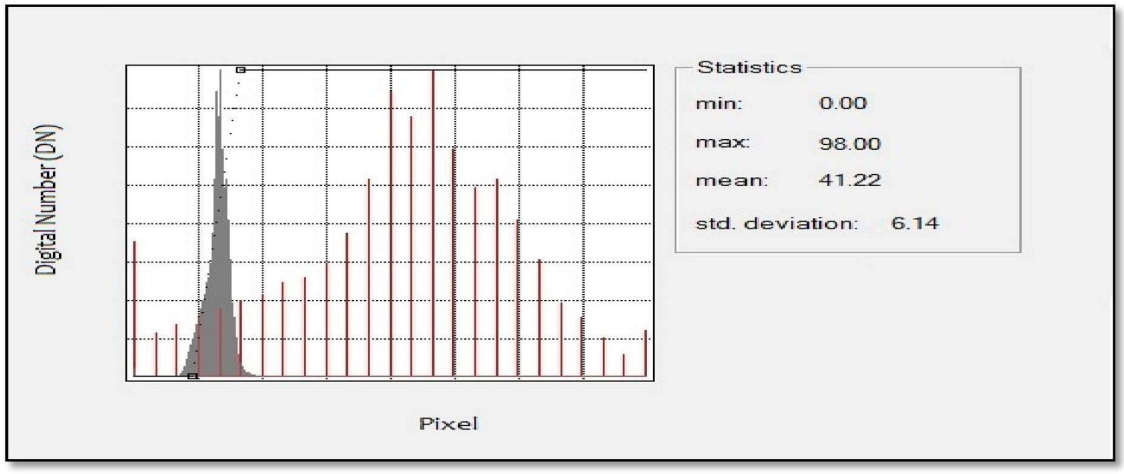

Fig: 38 Histogram Equalization of image in Red Band of 1980 of JCF.

The segmentation of pixel values shows the lowest reflectance 0.00 to max reflectance of 103 as digital numbers of pixels. Their standard deviation is 37.33 in green band of image. It depicts that the vegetation and other classes have clearer interpretations in the green bands.

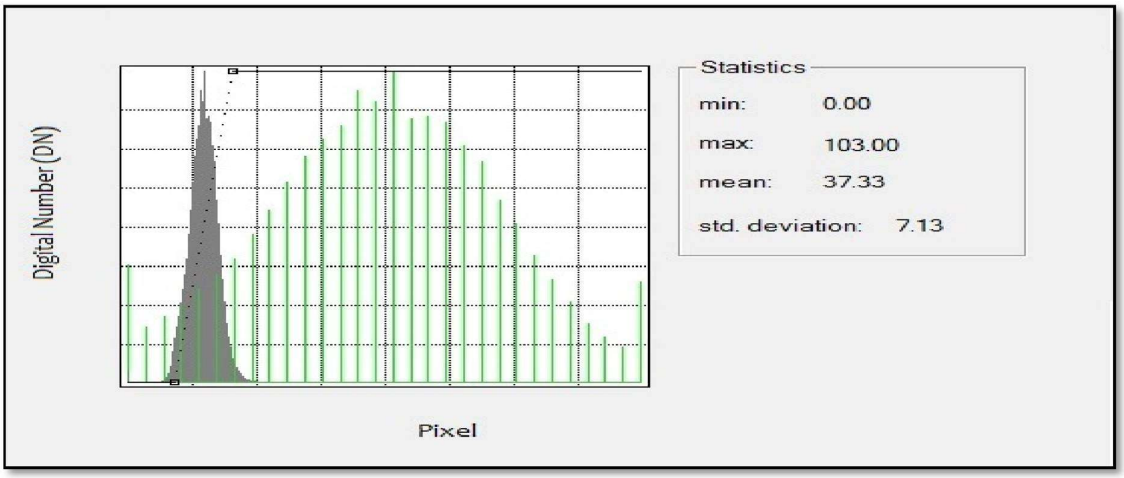

Fig: 39 Histogram Equalization of image in Green Band of 1980 of JCF

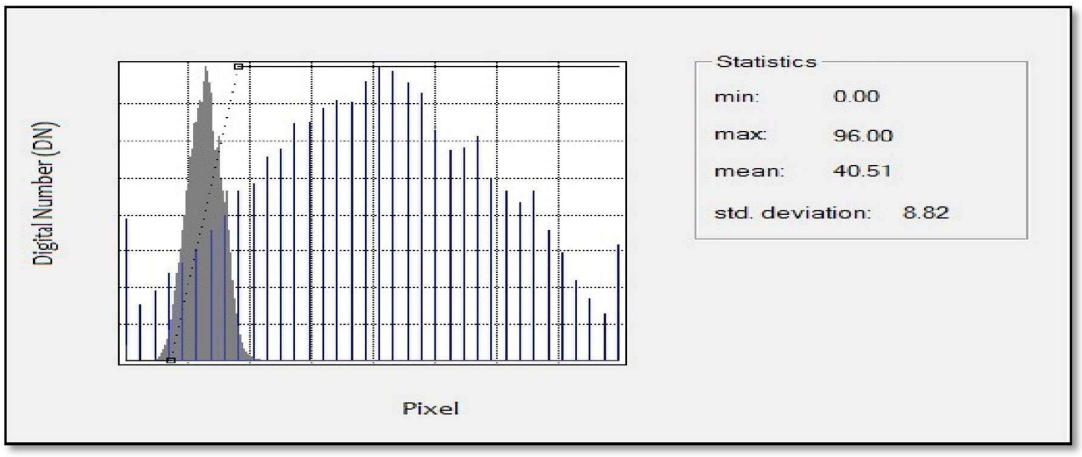

Fig: 40 Histogram Equalization of image in Blue Band of 1980 of JCF

The various bands of satellite image shows vegetation and CSF in different tones. The Histogram Equalization shows the segmentation of pixel values for better interpretations. The low vegetation cover shows peak and high vegetation cover shows non-peak regions.

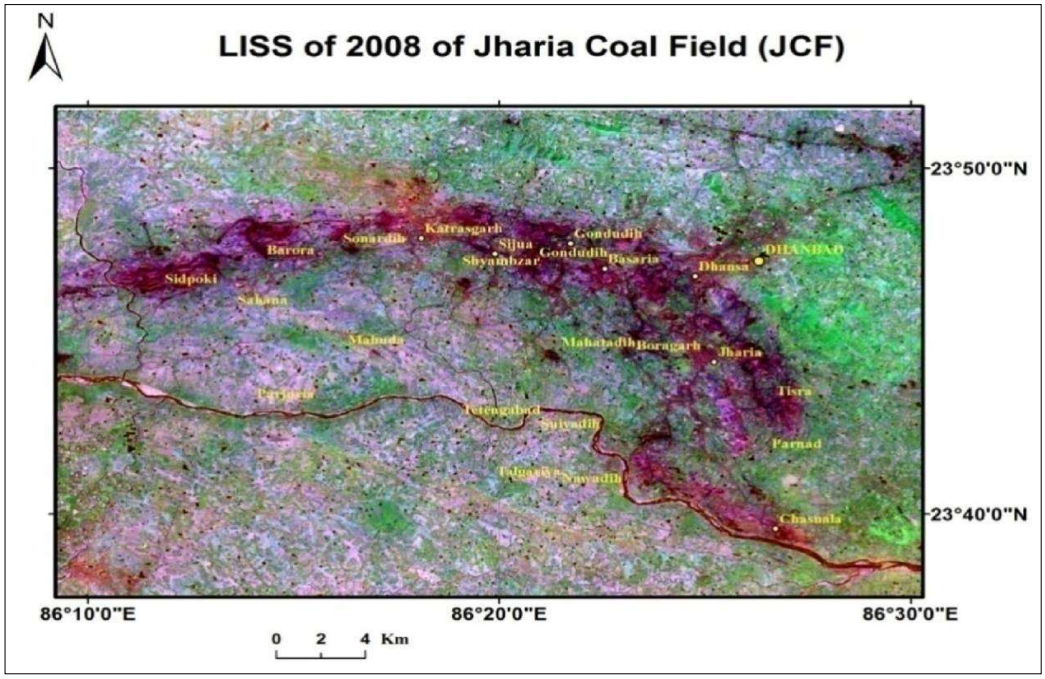

Fig: 41 LISS image of 2008 of JCF

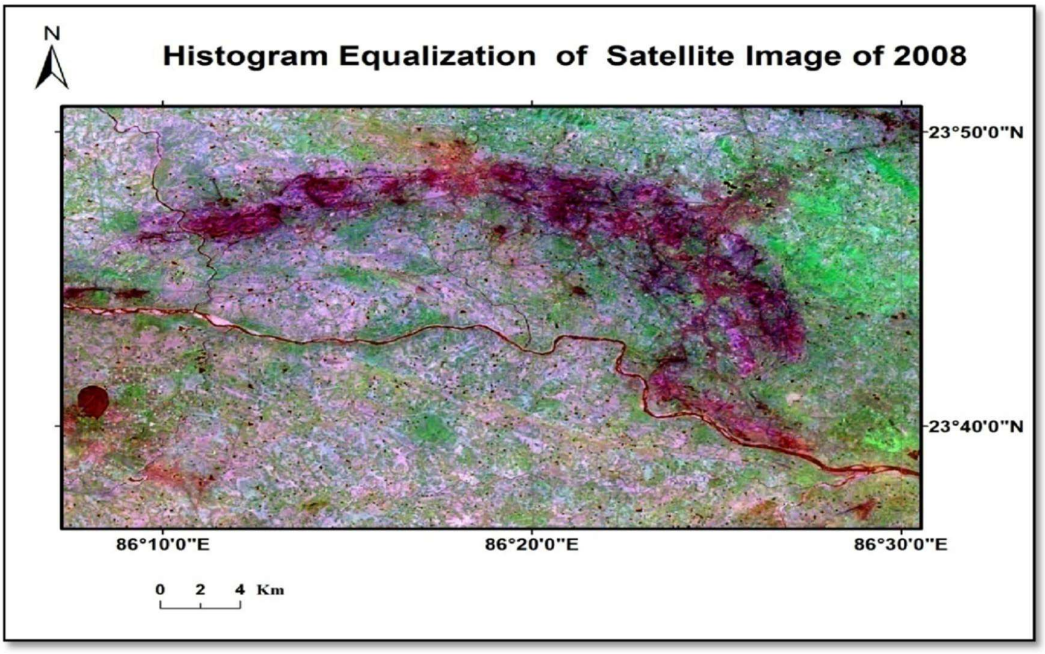

Fig: 42 Histogram Equalization image of 2008 of JCF

The segmentation of pixel values shows the lowest reflectance 0.00 to max reflectance of 107 as digital numbers of pixels. Their standard deviations were 6. 28 in red band of image. It depicts that the vegetation and the other classes were mixed in the red bands.

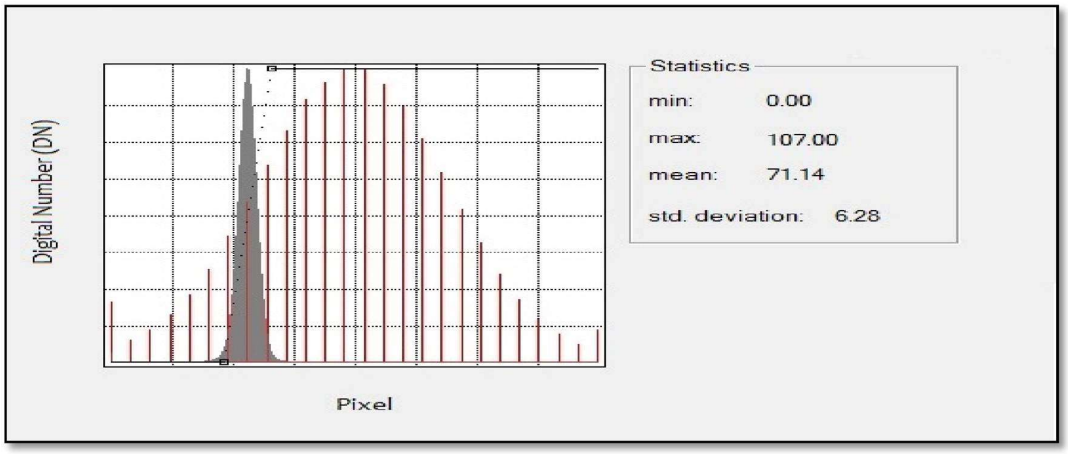

Fig: 43 Histogram Equalization of image in Red Band of 2008 of JCF

The segmentation of pixel values shows the lowest reflectance 0.00 to max reflectance of 119 as digital numbers of pixels. Their standard deviations were 8.28 in green band of image. It depicts that the vegetation and other classes were mixed in the red bands.

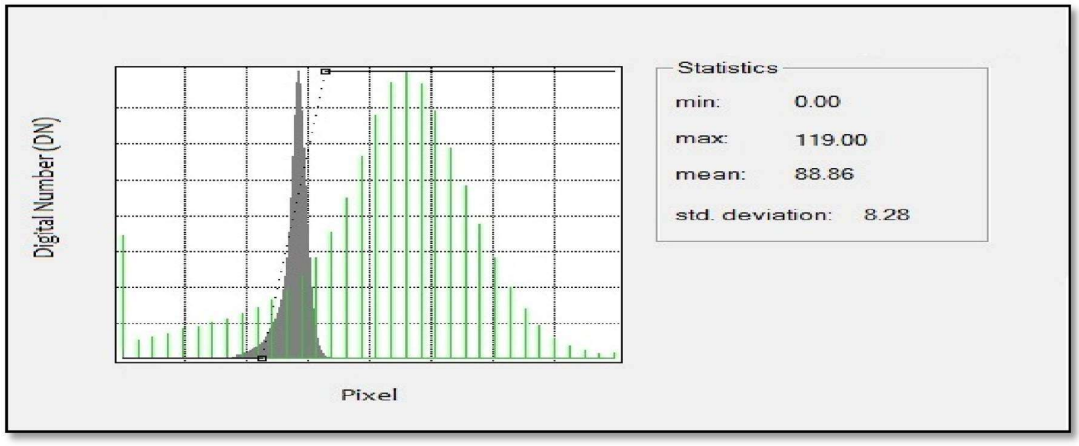

Fig: 44 Histogram Equalization of image in Green Band of 2008 of JCF

The segmentation of pixel values shows the lowest reflectance 0.00 to max reflectance of 131 as digital numbers of pixels. Their standard deviation is 84.77 in blue band of image. It depicts that the vegetation and other classes were mixed in the red bands.

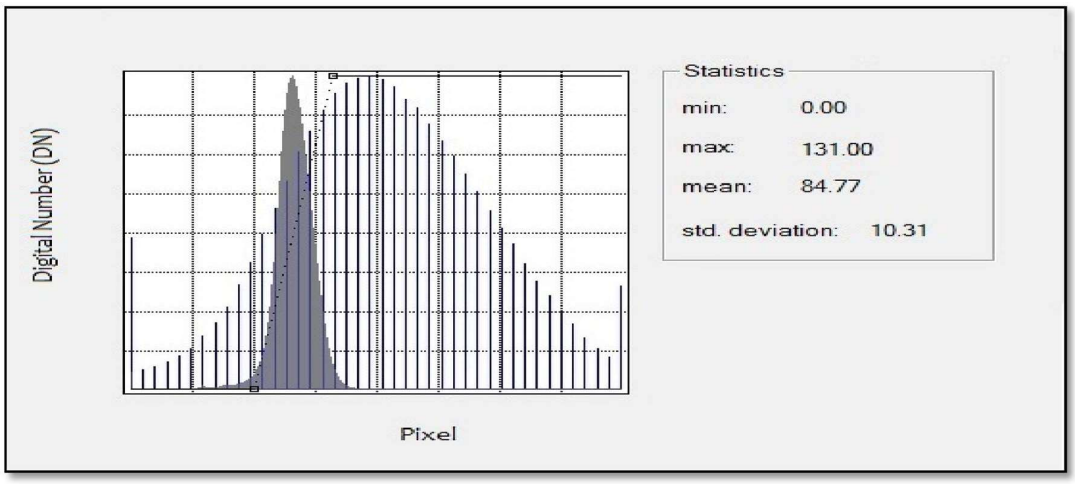

Fig: 45 Histogram Equalization of image in Blue Band of 2008 of JCF

The various bands of satellite image show vegetation and CSF in the different tones. The Histogram Equalization shows the segmentation of pixel values for better interpretations. The low vegetation cover shows peak and high vegetation cover shows non-peak regions.

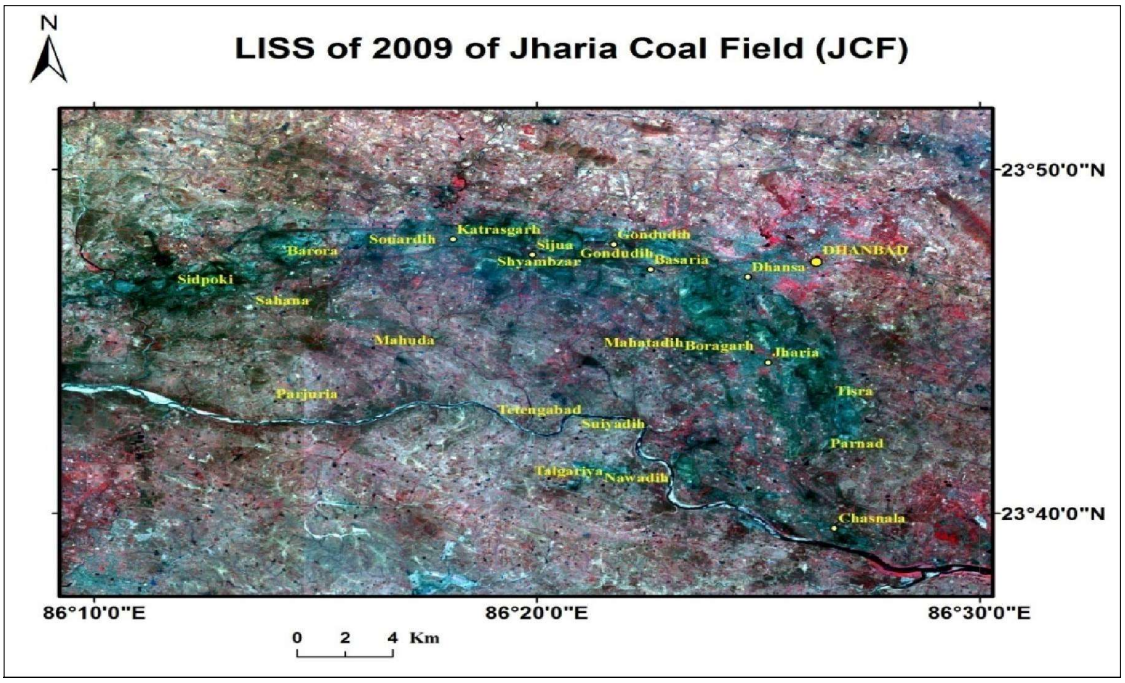

Fig: 46 LISS image of 2009 of JCF

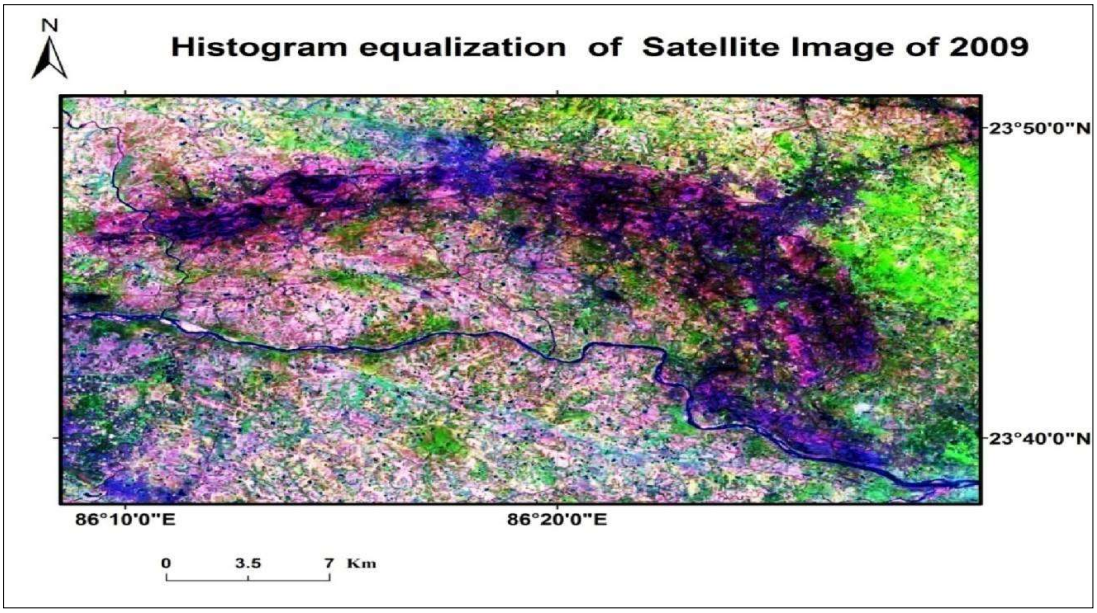

Fig: 47 Histogram Equalization image of 2009 of JCF

The segmentation of pixel values shows the lowest reflectance 37.0 to max reflectance of 107 as digital numbers of pixels. Their standard deviations were 5. 16 in blue band of image. It depicts that the vegetation and other classes were mixed in the red bands.

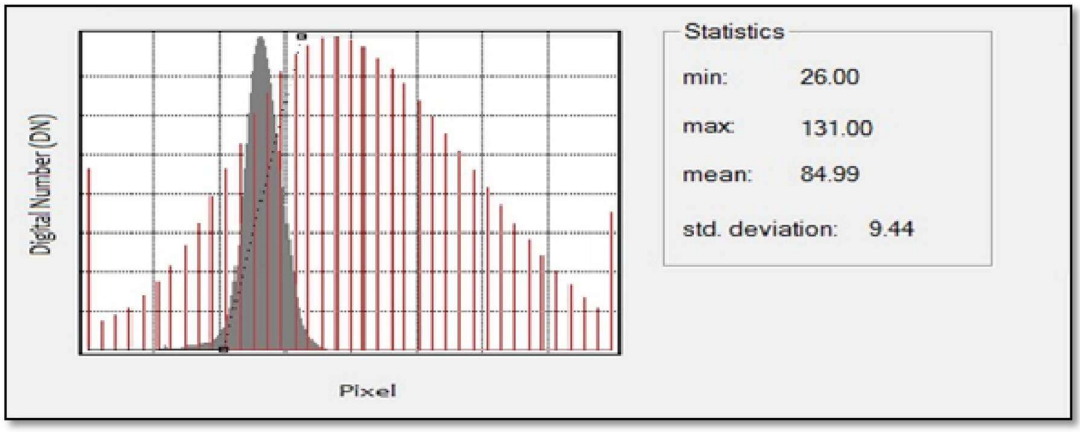

Fig: 48 Histogram Equalization statistics of image in Red Band of 2009 of JCF

The segmentation of pixel values show that the lowest reflectance 45.0 to max reflectance of 116 as digital numbers of pixels. Their standard deviations are 89.11 in red band of image. It depicts that the vegetation and other classes were mixed in the red bands.

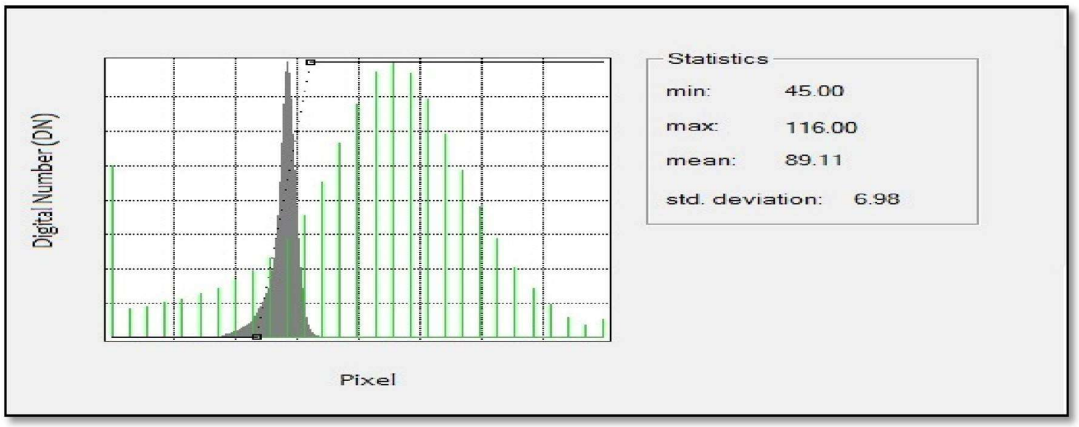

Fig: 49 Histogram Equalization statistics of image in Green Band of 2009 of JCF

The segmentation of pixel values shows the lowest reflectance 45.0 to max reflectance of 116 as digital numbers of pixels. Their standard deviation is 89.11 in blue band of image. It depicts that the vegetation and other classes were mixed in the red bands.

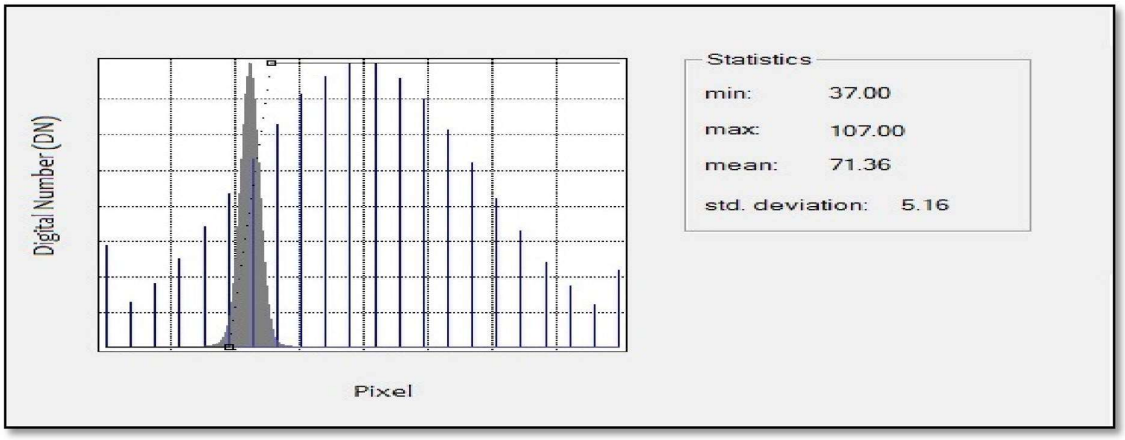

Fig: 50 Histogram Equalization statistics of image in Blue Band of 2009 of JCF

The various bands of satellite image show vegetation and CSF in different tones. The Histogram Equalization shows the segmentation of pixel values for better interpretations. The low vegetation cover shows peak and high vegetation cover shows non-peak regions.

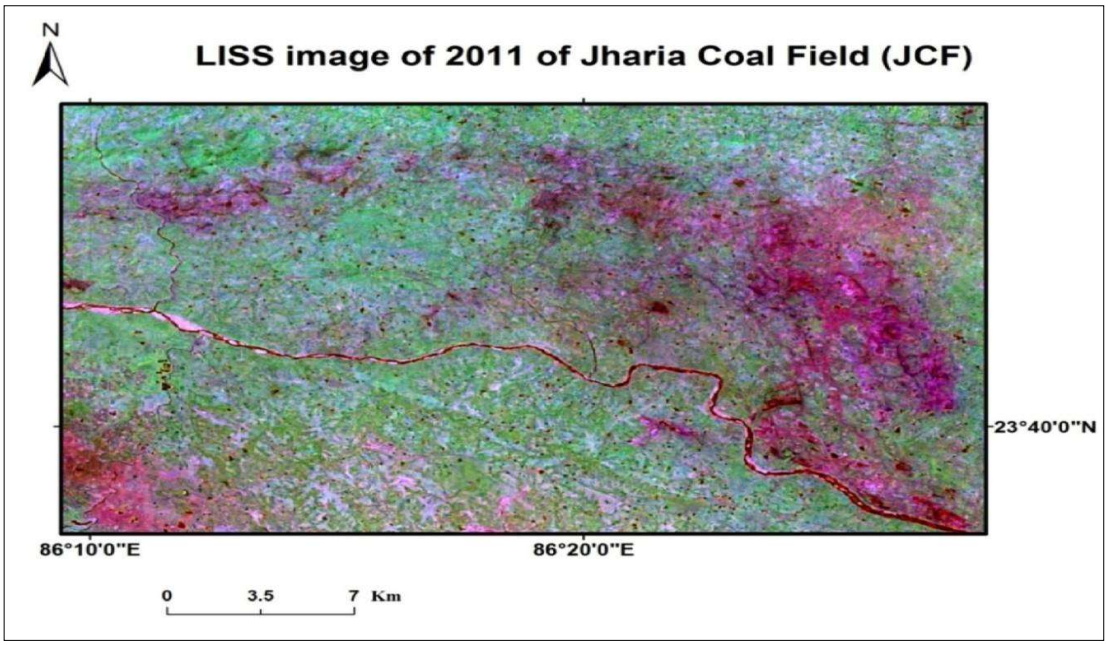

Fig: 51 LISS image of 2011 of JCF

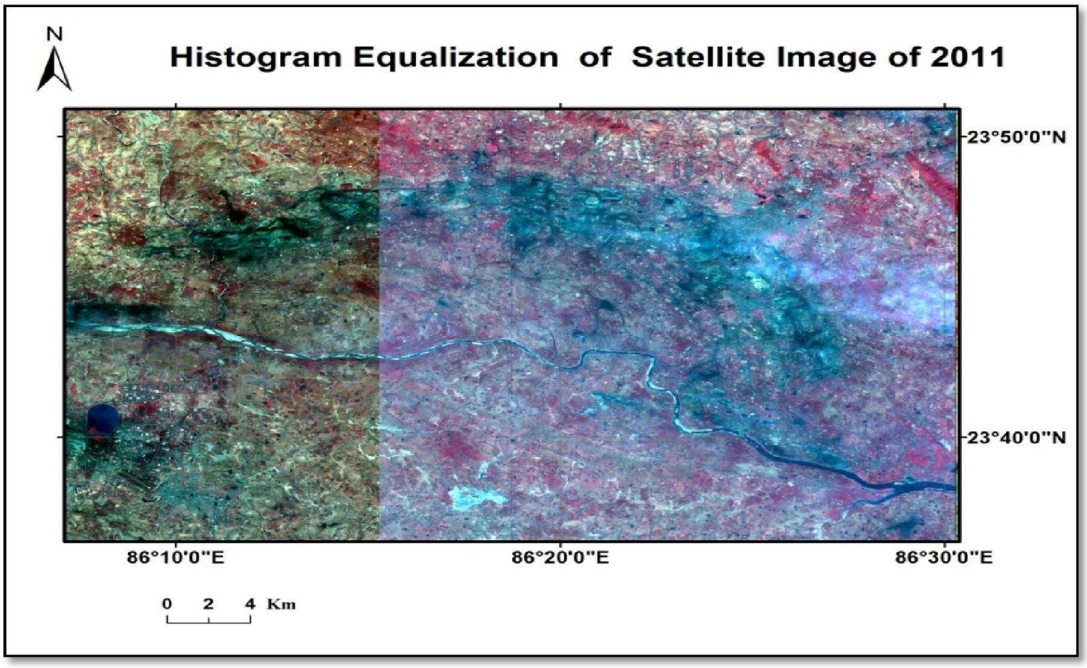

Fig: 52 Histogram Equalization image of 2011 of JCF

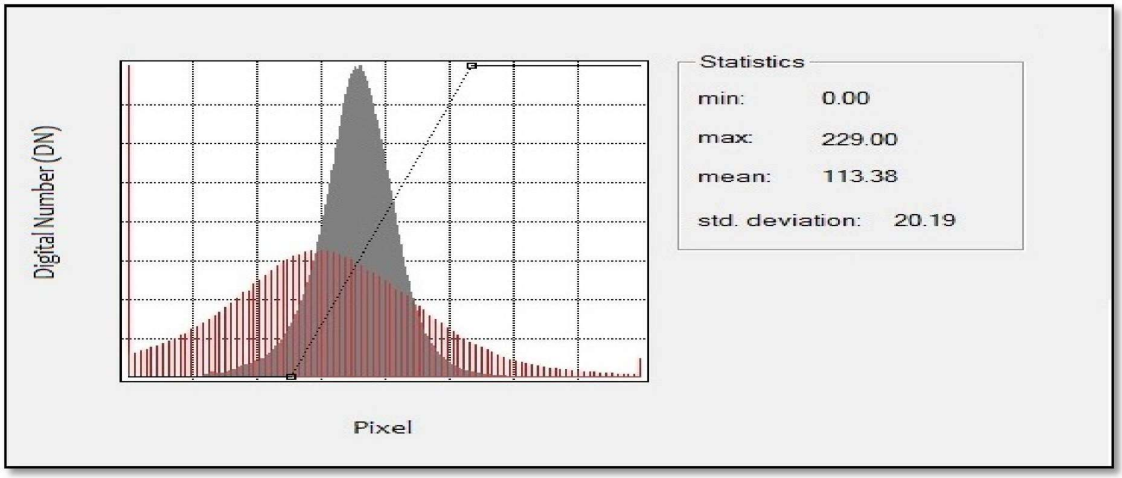

Fig: 53 Histogram Equalization of statistics of image in Red Band of 2011 of JCF

The segmentation of pixel values shows the lowest reflectance of 0.00 to max reflectance of 229 as digital numbers of pixels. Their standard deviation is 113.38 in red band of image. It depicts that the vegetation and other classes were mixed in the red bands.

The segmentation of pixel values shows the lowest reflectance 0.00 to max reflectance of 218 as digital numbers of pixels. Their standard deviations are 12.51 in red band of image. It depicts that the vegetation and other classes were mixed in the red bands.

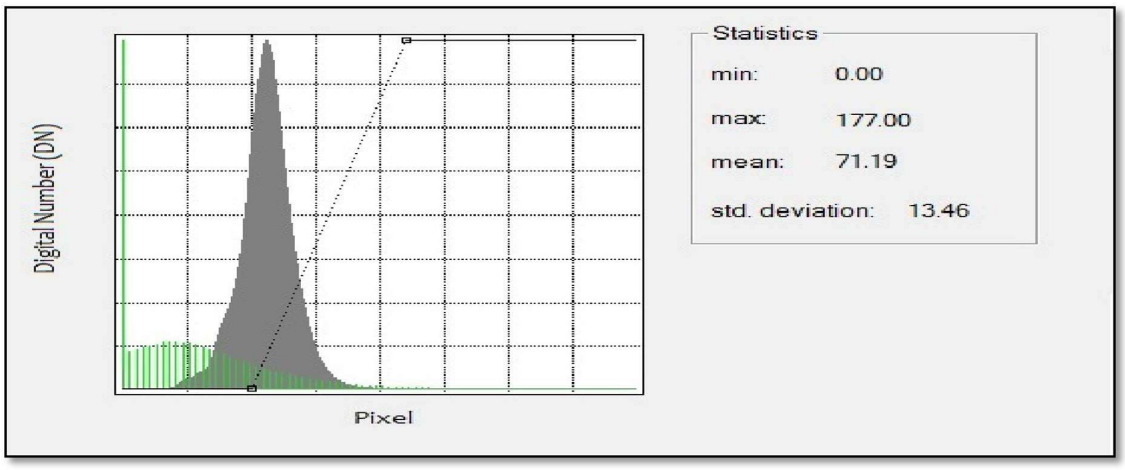

Fig: 54 Histogram Equalization statistics of image in Green Band of 2011 of JCF

The segmentation of pixel values shows the lowest reflectance 0.00 to max reflectance of 177 as digital numbers of pixels. Their standard deviation was 13.46 in green band of image. It depicts that the vegetation and other classes were mixed in the red bands.

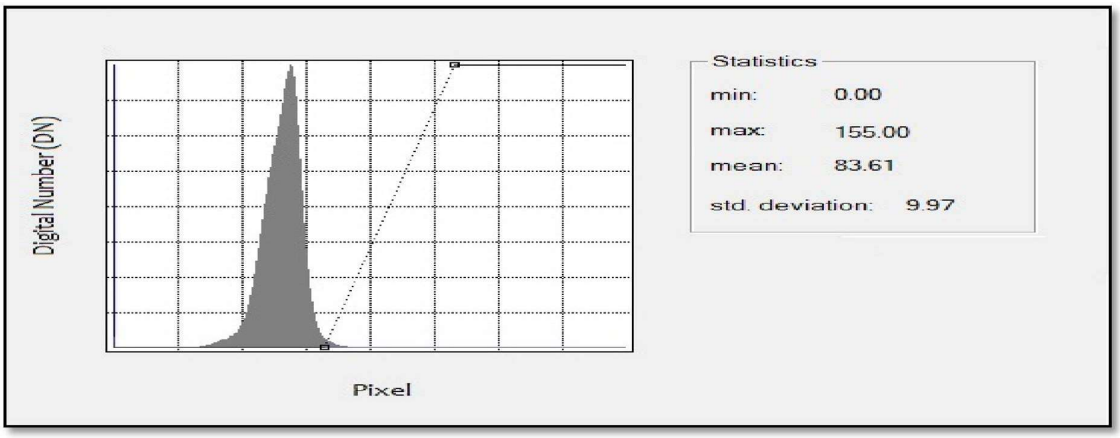

Fig: 55 Histogram Equalization statistics of image in Blue Band of 2011 of JCF

The various bands of satellite image shows vegetation and CSF in different tones. The Histogram Equalization shows the segmentation of pixel values for better interpretations. The low vegetation cover shows peak and high vegetation cover shows non-peak regions.

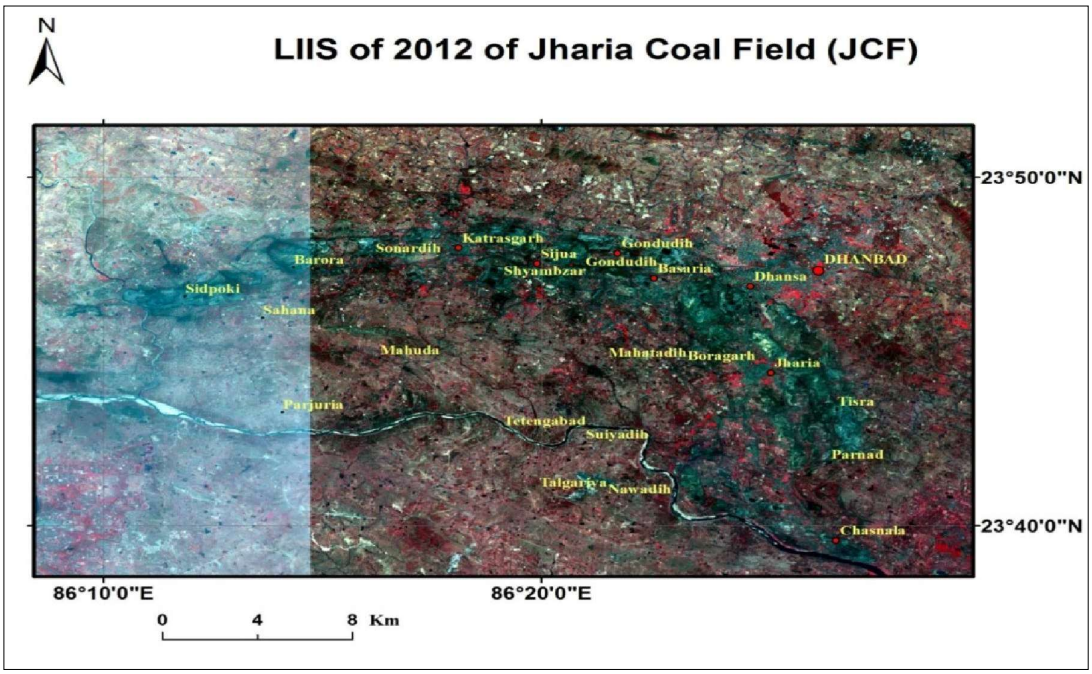

Fig: 56 LISS image of 2012 of JCF

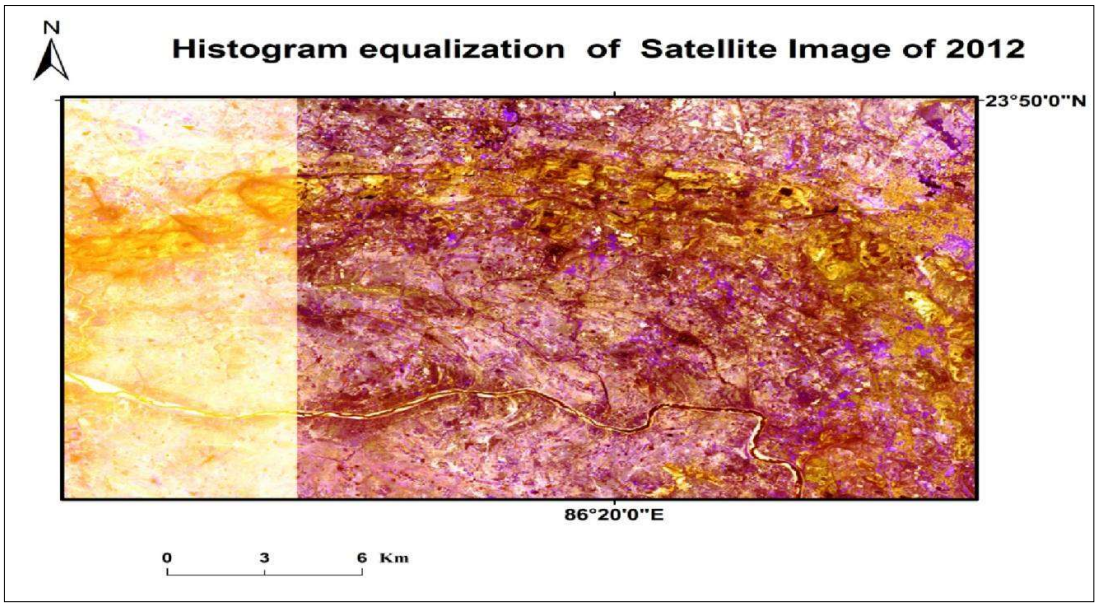

Fig: 57 Histogram Equalization image of 2012 of JCF

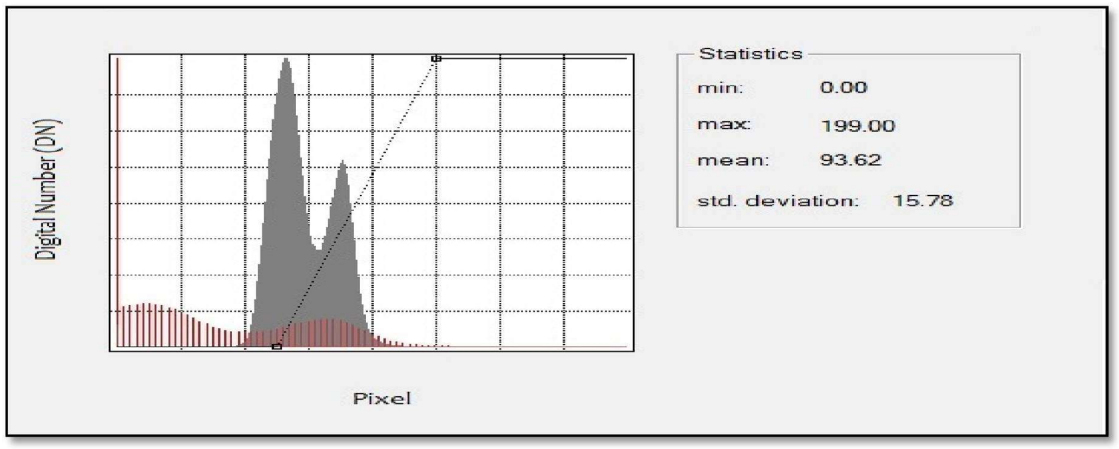

Fig: 58 Histogram Equalization of statistics of image in Red Band of 2012 of JCF

The segmentation of pixel values shows the lowest reflectance 0.00 to max reflectance of 199 as digital numbers of pixels. Their standard deviation is 15. 78 in the red band of images. It depicts that the vegetation and the other classes were mixed in the red bands.

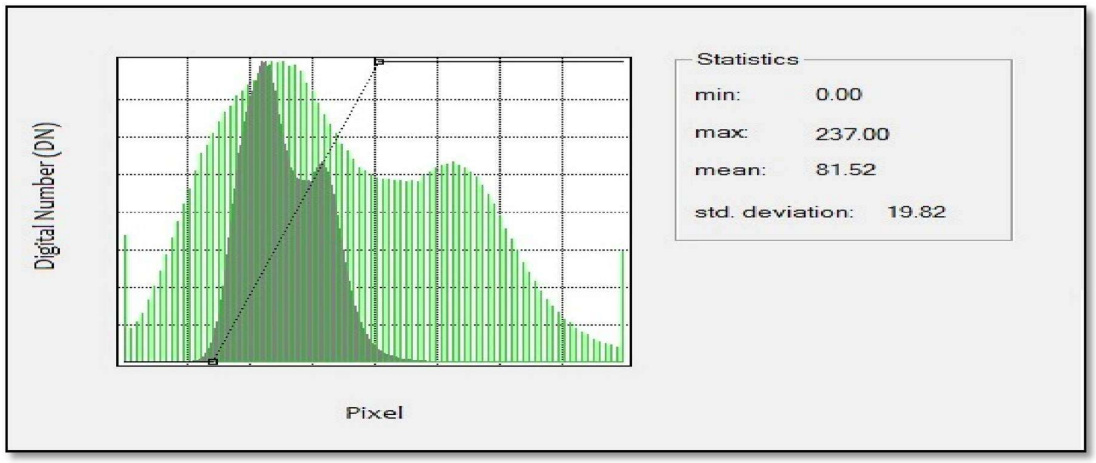

Fig: 59 Histogram Equalization statistics of image in Green Band of 2012 of JCF

The segmentation of pixel values shows the lowest reflectance 0.00 to max reflectance of 237 as digital numbers of pixels. Their standard deviations were 19.82 in red band of image. It depicts that the vegetation and other classes were mixed in the green bands.

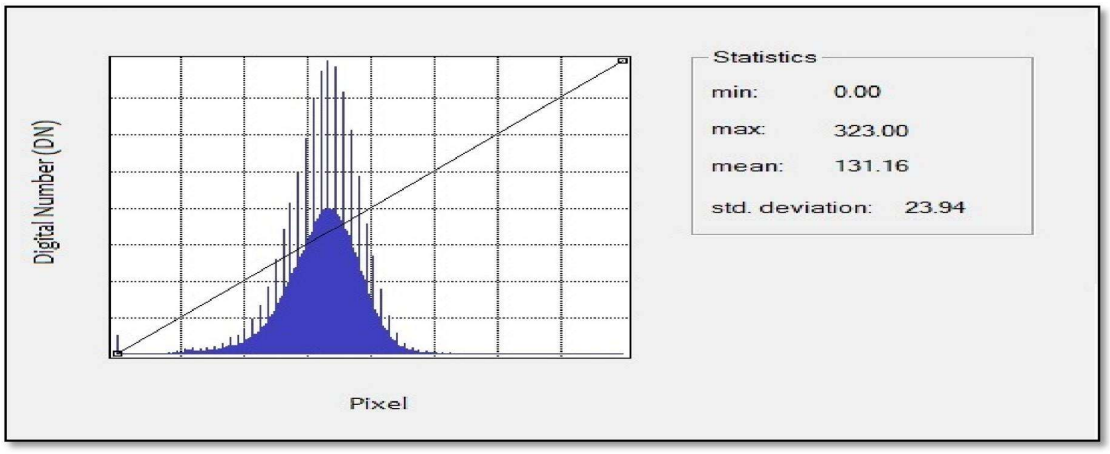

Fig: 60 Histogram Equalization statistics of image in Blue Band of 2012 of JCF

The various bands of satellite image shows vegetation and CSF in different tones. The Histogram Equalization shows the segmentation of pixel values for better interpretations. The low vegetation cover shows peak and high vegetation cover shows non-peak regions.

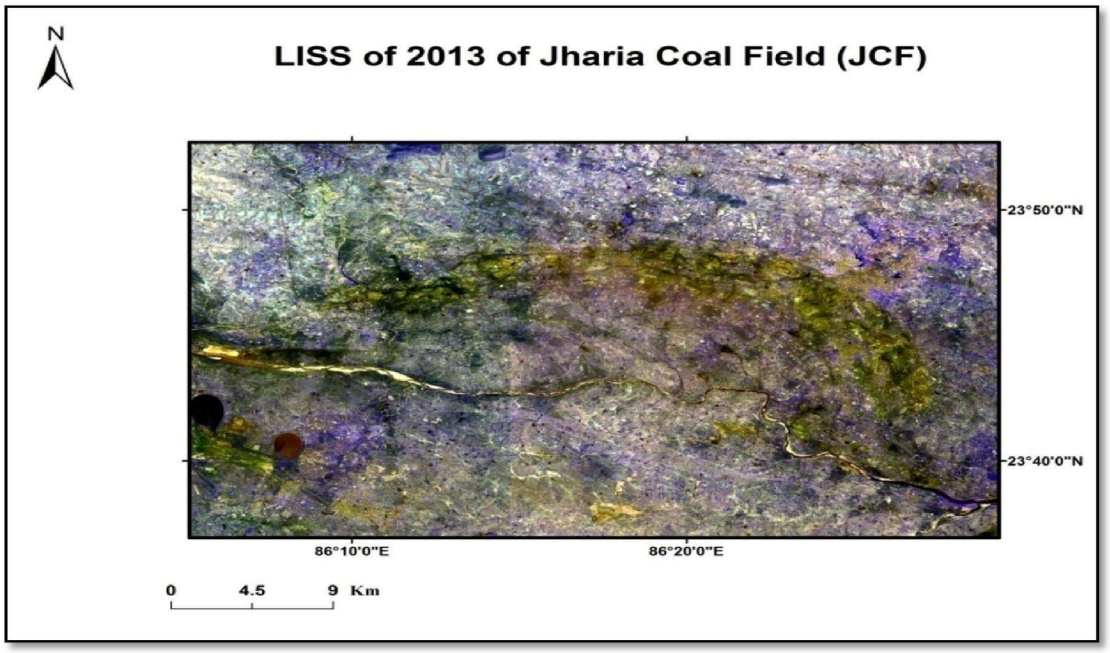

Fig: 61 LISS image of 2013 of JCF

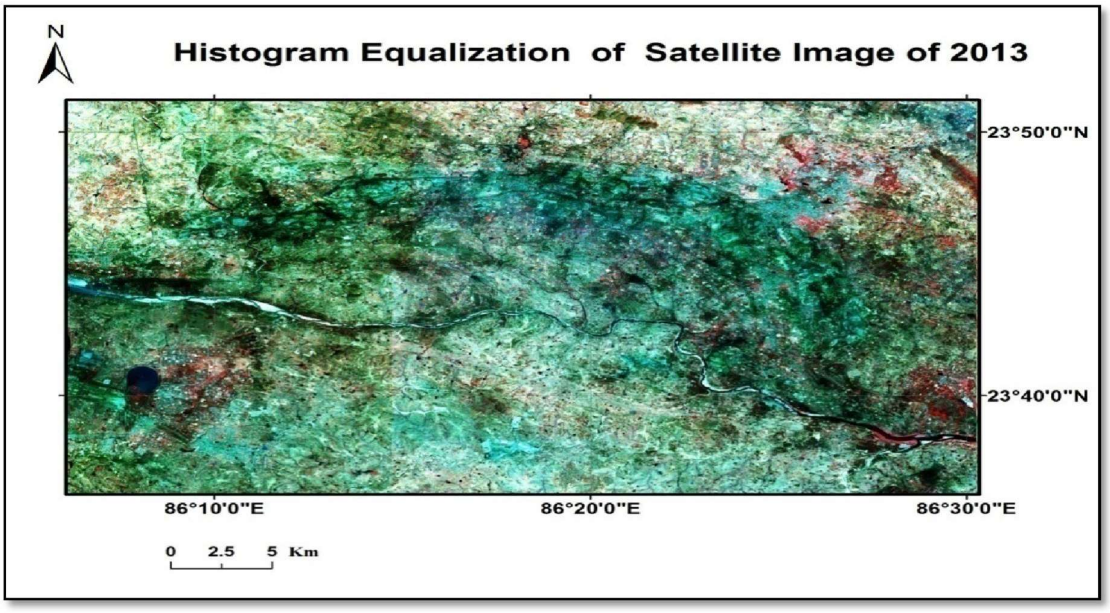

Fig: 62 Histogram Equalization image of 2013 of JCF

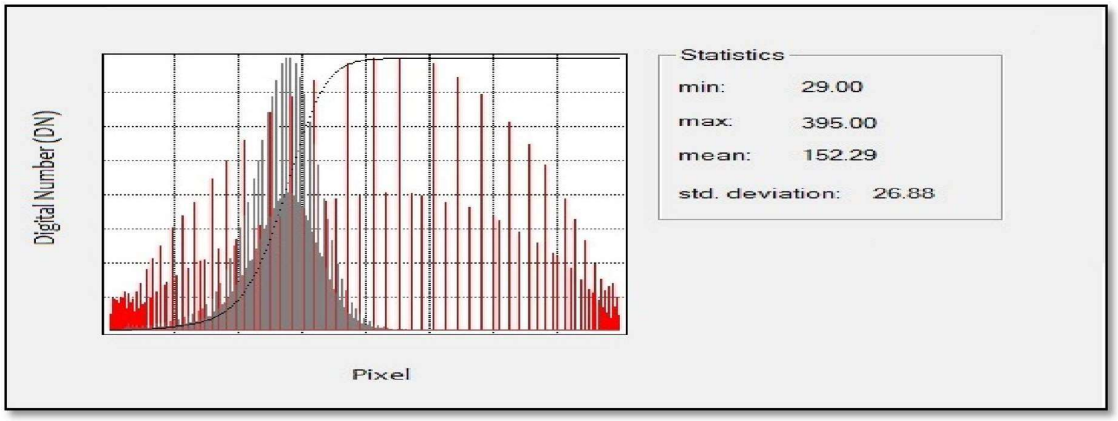

Fig:63 Histogram Equalization of statistics of image in Red Band of 2013 of JCF

The segmentation of pixel values shows the lowest reflectance 0.00 to max reflectance of 395 as digital numbers of pixels. Their standard deviations were 26.88 in red band of image. It depicts that the vegetation and other classes were mixed in the red bands.

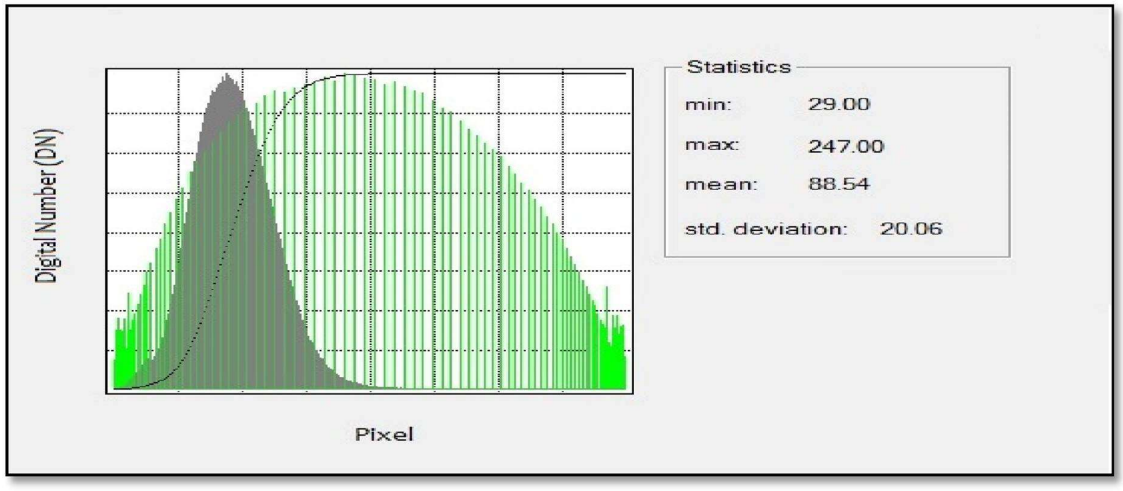

Fig: 64 Histogram Equalization statistics of image in Green Band of 2013 of JCF

The segmentation of pixel values shows the lowest reflectance 29.00 to max reflectance of 247 as digital numbers of pixels. Their standard deviations were 12.51 in green band of image. It depicts that the vegetation and other classes were mixed in the green bands.

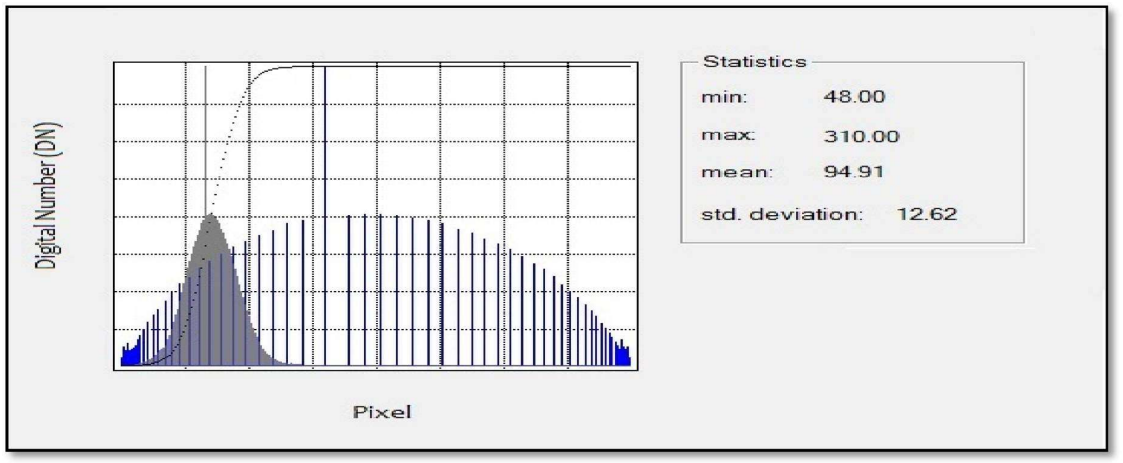

Fig: 65 Histogram Equalization statistics of image in Blue Band of 2013 of JCF

The segmentation of pixel values shows the lowest reflectance 48.00 to max reflectance of 310 as digital numbers of pixels. Their standard deviations are 94.91 in blue band of image. It depicts that the vegetation and other classes were mixed in the blue bands.

3.5 CLASSIFICATION PARAMETRIC TECHNIQUES – IMAGE SEGMENTATION

The quantitative analysis of the data sets in data mining, image segmentation and pattern are mix methods of traditional and advanced algorithms. The aim of segmentation grouping is to classify the image into homogenous regions based on the pixel characteristics. The data mining deploys many different algorithms techniques. These algorithms were classified into seven types namely:

i. Level Slicing,

ii. Thresholding,

iii. Edge detection,

iv. Region based segmentation,

v. Template matching,

vi. K- Mean and

vii. Maximum Likelihood

Remote sensing and GIS are routinely used as a decision support tool in a variety of applications. Digital enhancement of remote sensing images, particularly image segmentation and classification, are very useful for mapping the spatial distributions of soils, vegetation, water bodies, coal and fires, and other land cover types. A time series of land cover maps serves as a powerful basis for making decisions related to land and coal fire management. Surface attributes were delineated from the Satellite imagery, DEM and Toposheets. Landuse vegetation data characteristics were influenced by infiltration, erosion and evapo-transpiration. The classification arranged the pixels of image on the basis of spectral digital numbers within different bands. The pixel indices comprised of the greenness, rainfall, infiltration, water availability and underground conditions and they provided texture or pattern associated with the objects. The classification based on the pixels' radiation or their reflectance property.

In pixel based approach, each pixel is classified on the basis of the digital numbers. These digital numbers are the associations of the texture statistics derived from the satellite imagery as attributes of the land cover classifications for the CSF.

3.5.1 K-MEANS CLUSTERING ALGORITHM

3.5.1.1 K – MEAN IN ERDAS IMAGINE SOFTWARE.

The K mean cluster is applied for the image of the area. The total 25 classes have been given to 2008491 pixels. The maximum numbers of pixels were in class 17 and minimum numbers of the pixels were in class 21. The digital value cluster formed by K means methods are provided in the table below.

Table: 8 Percentage pixels in classes by K- Mean Methods

S. No	Class	Pixels	Percentage (%)
1	Class1	44235	2.202399712
2	Class2	82532	4.109154584
3	Class3	81651	4.065290808
4	Class4	54531	2.715023368
5	Class5	85942	4.278933787
6	Class6	52792	2.628440954
7	Class7	94951	4.727479486
8	Class8	82542	4.10965247
9	Class9	84714	4.217793358
10	Class10	63687	3.170887995
11	Class11	104059	5.180954259
12	Class12	95194	4.739578121
13	Class13	96028	4.781101832
14	Class14	89941	4.478038488
15	Class15	107920	5.37318813
16	Class16	71442	3.556998762
17	Class17	105776	5.266441323
18	Class18	94600	4.710003679
19	Class19	76283	3.798025483
20	Class20	64348	3.203798274
21	Class21	41826	2.082458921

22	Class22	50338	2.506259675
23	Class23	83628	4.163722914
24	Class24	105016	5.22860197
25	Class25	94515	4.705771646
Total		**2008491**	**100**

3.5.1.2 K – Mean in SPSS software.

The number of cluster is 25 and the initial cluster centres were evaluated based on the available data. The initial cluster is provided in the table. These were vectors with their value depending on 4 variables. The first iteration which joins the centre is updated. The iteration process of redistribution of units stops whenever there is no change in cluster centres. The results of these analyses were summarized in the table : 9 given below.

Table: 9 Initial Cluster Centres

	Band 1	Band 2	Band 3	Band 4
1	13728	85048	3469	53931
2	12	819	1267	370
3	139655	15421	6905	94226
4	443	595	65175	2464
5	93301	40672	3823	109935
6	52081	51126	3443	82933
7	5799	103501	2858	42435
8	166911	23933	5332	70724
9	99712	11452	8265	68810
10	117055	35245	4214	62370
11	153580	27741	4896	146785
12	28630	65064	3310	68052
13	30	96	33898	530
14	169154	20891	5775	130133
15	8	59720	1106	6594
16	80993	9784	8966	30252
17	40989	6404	12075	41698
18	3583	112769	2647	18906
19	20545	76205	3384	30138
20	52236	7331	10870	22945
21	118886	13205	7502	41067
22	70	91057	1482	22412
23	39036	57320	3348	38624
24	71570	45864	3743	48675
25	65527	8561	9759	54388

Table: 10 Change in Cluster Centres

	1	3	4	5	6	7
1	0	0	0	0	0	0
2	2.15E+03	261.18	188.4	0	0	0
3	0	0	0	0	0	0
4	5.69E+03	692.457	0	0	0	0
5	0	0	0	0	0	0
6	0	0	0	0	0	0
7	6.04E+03	0	3.22E+03	0	0	0
8	9.04E+03	0	0	0	0	0
9	0	0	0	0	0	0
10	0	0	0	0	0	0
11	8.13E+03	0	0	0	0	0
12	0	0	0	0	0	0
13	7.30E+03	1.61E+03	0	1.05E+03	1.07E+03	0
14	0	0	0	0	0	0
15	9.56E+03	3.05E+03	2.71E+03	0	0	0
16	0	0	0	0	0	0
17	1.55E+04	3.75E+03	5.81E+03	2.74E+03	2.43E+03	0
18	6.07E+03	2.93E+03	3.39E+03	0	0	0
19	0	0	0	0	0	0
20	9.94E+03	0	6.93E+03	0	0	0
21	0	0	0	0	0	0
22	5.78E+03	3.18E+03	0	0	0	0
23	0	0	0	0	0	0
24	0	0	0	0	0	0
25	0	0	0	0	0	0

The clusters of pixel changes from initial to final clusters are shown in table below.

Table: 11 Final Cluster Centres

	Band 1	Band 2	Band 3	Band 4
1	13728	85048	3469	53931
2	12	819	1267	370
3	139655	15421	6905	94226
4	623	549	5783	4217
5	93301	40672	3823	109935
6	52081	51126	3443	82933
7	2659	106222	2270	35104
8	164366	20875	5762	62616
9	99712	11452	8265	68810
10	117055	35245	4214	62370
11	146256	29836	4720	143949
12	28630	65064	3310	68052
13	1699	782	3151	5083
14	169154	20891	5775	130133
15	2	35927	750	6618
16	80993	9784	8966	30252
17	15126	3430	2006	22228
18	1559	105828	2088	15880
19	20545	76205	3384	30138
20	42070	6411	1210	27891
21	118886	13205	7502	41067
22	2282	84284	1792	17762
23	39036	57320	3348	38624
24	71570	45864	3743	48675
25	65527	8561	9759	54388

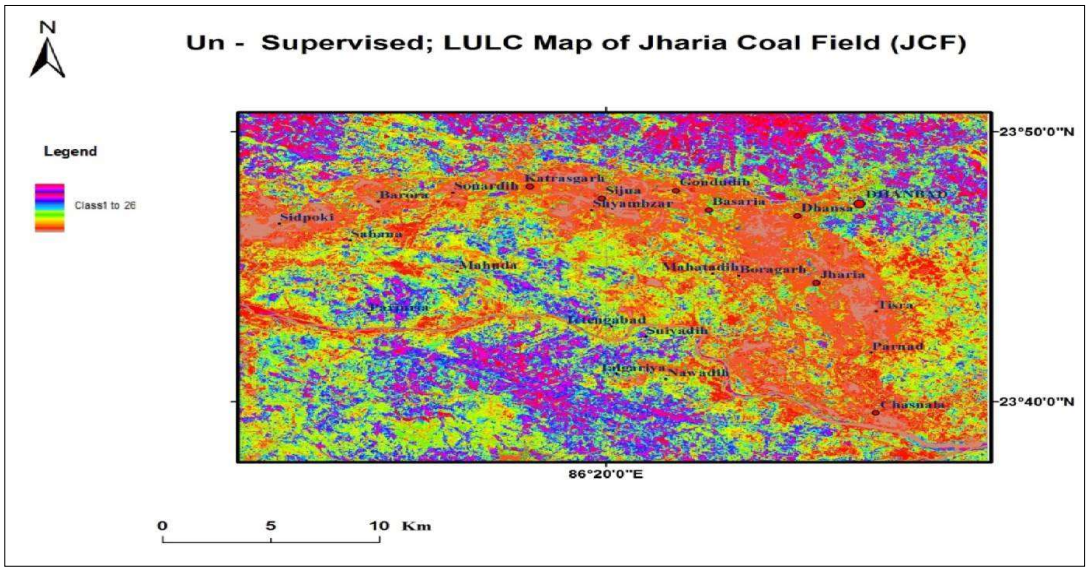

Fig: 66 Un supervised results of pixels JCF

3.5.2 ML CLASSIFICATION

ML Classification derived from the Bayes theorem equation number (3) states that a posteriori distribution P (i|¢), is often treated as a normalization i.e., the probability that a pixel with feature vector ¢ belongs to classification, is given by:

$$P(i|¢)=P(¢|i)P(i)/P(¢) \ / \ P(¢) \qquad \text{..... Eq.3}$$

where, P (¢|i) is the likelihood function, P (i) is the a priori information P (¢) is the probability.

The pre-classified values of the target variables are the training set of data. A data mining pattern is constructed using the training samples provided in the training data set. The value of the target variable is hidden temporarily from the models, performs classification according to the patterns and structure it learnt from the training set. The efficacies of the classifications are then evaluated by comparing them against the true values of the target variable.

MLC is an application of supervised models. The pixel values are assumed for various classes. The methods apply to simulate image data and our experimental results to the proposed model could improve the supervised MLC segmentation results when there are considerable differences across subjects. ML classification method is based on the Bayes theorem. The vector and the matrix are the input functions and can be estimated from the training pixels of class. Here, ML was used to classify a diverse tropical land covers recorded from the Resourcesat I satellite through maximum likelihood classifier.

3.5.2.1 ML classification using ERDAS Imagine software.

Image classified in ERDAS by supervised classification

Table: 12 percentage of pixels in 25 classes in MLC

S. No	Class	Pixels	Percentage (%)
1	Class1	1129	0.05621135
2	Class2	98321	4.89526714
3	Class3	28875	1.43764647
4	Class4	2520	0.12546733
5	Class5	22527	1.1215883
6	Class6	18938	0.94289693
7	Class7	75	0.00373415
8	Class8	127056	6.32594321
9	Class9	31098	1.54832658
10	Class10	13545	0.67438689
11	Class11	28724	1.43012839
12	Class12	69211	3.44592035
13	Class13	67003	3.33598707
14	Class14	12586	0.6266396
15	Class15	44185	2.19991028
16	Class16	26125	1.30072776
17	Class17	691039	34.4058798
18	Class18	6078	0.30261525
19	Class19	154536	7.69413455
20	Class20	10435	0.51954427
21	Class21	17521	0.87234645
22	Class22	8550	0.42569272
23	Class23	55017	2.73922064
24	Class24	402112	20.0206025
25	Class25	71285	3.54918195
		2008491	100

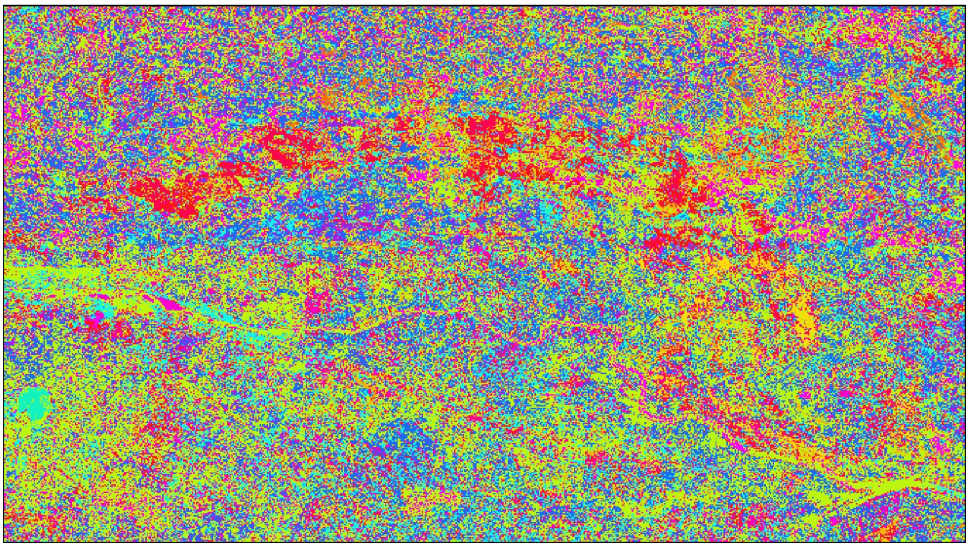

Fig.67: Supervised Image after applying maximum likelihood algorithms

3.5.2.2 ML classification through SPSS software

The pixel values were classified into supervised classifications (Fig :67) and the SPSS software was used for the supervised classification. The lowest mean was for the Band 4 and the lowest standard deviation was estimated in the Band 3.

Table: 13 Descriptive Statistics of data

	Mean	Std. Deviation	Analysis N	Missing N
Band1	1.12E+04	27926.712	255	76
Band2	1.02E+04	21666.372	255	58
Band3	7898.56	16733.643	255	1
Band4	7867.58	21604.899	255	0

Table: 14 Variance Analysis of pixels

Factor	Initial Eigen values			Extraction Sums of Squared Loadings		
	Tot	% of	Cumulative	Total	% of	Cumulative %
1	2.0	50.698	50.698	1.791	44.782	44.782
2	1.0	26.594	77.292	0.997	24.936	69.718
3	0.8	20.092	97.384			
4	0.1	2.616	100			
Extraction Method: Maximum Likelihood.						

Table: 15 Correlation Matrix

		Band1	Band2	Band3	Band4
Correlation	Band1	1	0.175	-0.066	0.849
	Band2	0.175	1	-0.15	0.415
	Band3	-0.066	-0.15	1	0.028
	Band4	0.849	0.415	0.028	1
Sig tailed)	Band1		0.009	0.19	0
	Band2	0.009		0.018	0
	Band3	0.19	0.018		0.328
	Band4	0	0	0.328	
a. Determinant = 0.181					

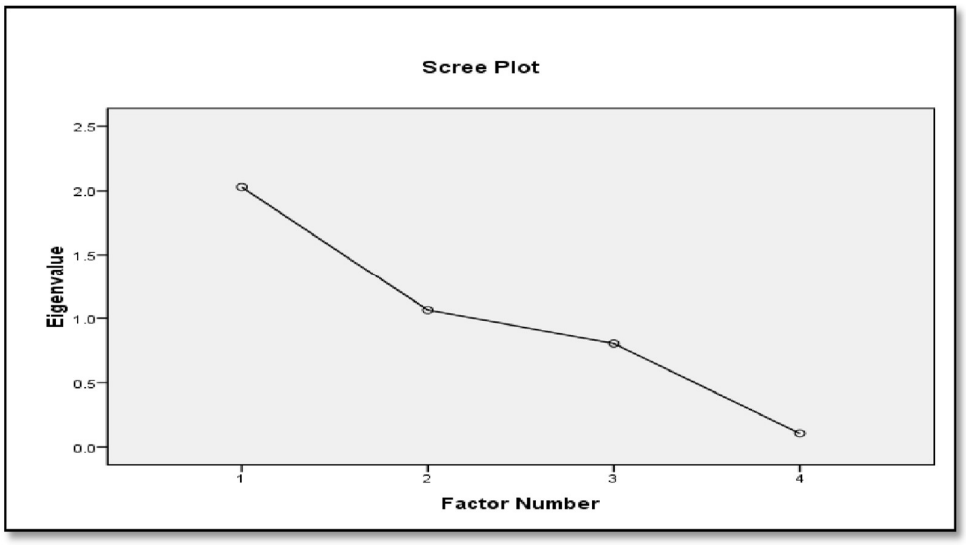

Fig.68: Scree plot between Eigen value and Factor Number

Table: 16 Reproduced Correlations

		Band1	Band2	Band3	Band4
Reproduced Correlation	Band1	.759a	0.175	0.058	0.849
	Band2	0.175	.999a	-0.15	0.415
	Band3	0.058	-0.15	.032a	0.028
	Band4	0.849	0.415	0.028	.999a
Residual	Band1		-2.50E- 05	-0.124	1.39E-05
	Band2	-2.50E-05		0	1.09E-07
	Band3	-0.124	0		0
	Band4	1.39E-05	1.09E-07	0	
Extraction Method: Maximum Likelihood.					
ka. Reproduced communalities					
b. Residuals are computed between observed and reproduced correlations. There are 1 (16.0%) no redundant Residuals with absolute values greater than 0.05.					

A plot shown in Fig: 68, displays the Eigen values associated with a component or factor in descending order versus the number of the component or factor. A plot can be used in principal components analysis and factor analysis to visually assess which components or factors explain most of the variability of the data mining of the data.

3.6 PRINCIPAL COMPONENT ANALYSIS

The Principal Component Analysis (PCA) is an application of digital processing of multispectral satellite images. PCA is covariance technique used to reduce a correlated multivariate measurements to pixels uncorrelated to each other. PCA applications are used to enhance an image particularly in the LULC classification of multispectral satellite images, where such images are used for increasing the interpretability and refining accuracy of the classification. The multispectral imagery and the reduction of the dimensionality is a key point for data analysis. The techniques of PCA have been transformation in digital image processing of multispectral satellite images where a number of correlated bands of the image data have been reduced to few uncorrelated bands. The refined image was used for ground truth validation in classification or image segmentation techniques of LULC interpretations.

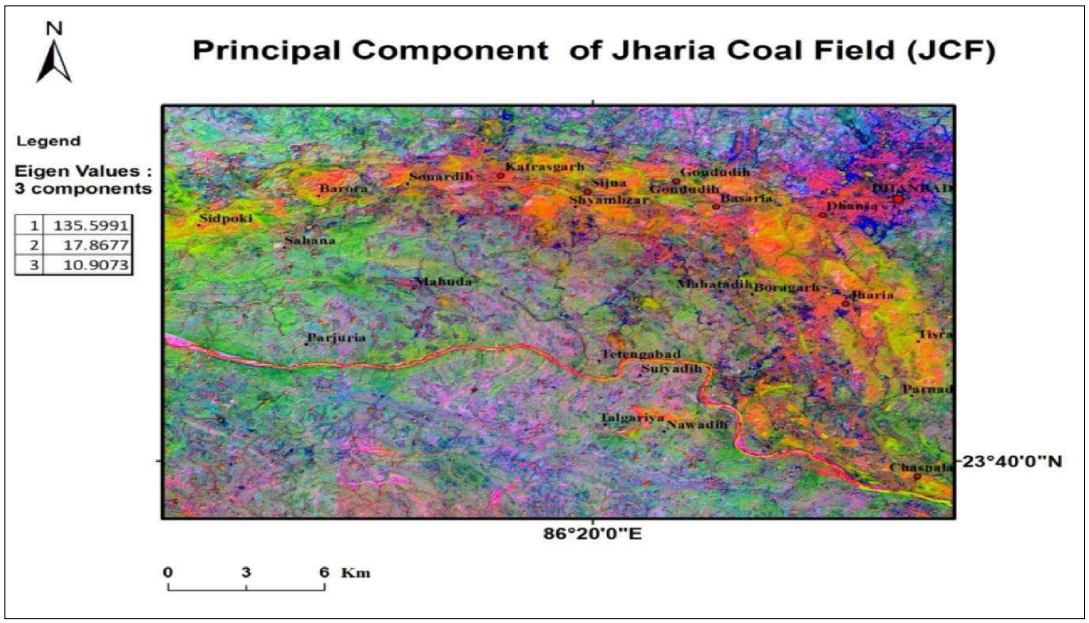

Fig.69: PCA image of JCF

3.7 VALIDATION OF MODEL

Ground truths and pixel sampling by high resolution image with point data were used to validate the classification result with the help of hand held GPS (Global Positioning System) of 3m accuracy. The models of pixels matrix values were obtained through data mining segmentation and validated in the field (model in Fig: 70). The accuracy assessment of the map was done by the ground truths control points. The ground truth positions were imposed over 30m DEM (Digital Elevation Model) of SRTM (Shuttle Radar Topography Mission) USGS (United States Geological Survey). The accuracy of landuse class type to the classification map was 80%. The accuracy increased by about 12% on applying the maximum likelihood classification method on the data under study. The ground truth and and verification data in table 17, 18 & 19.

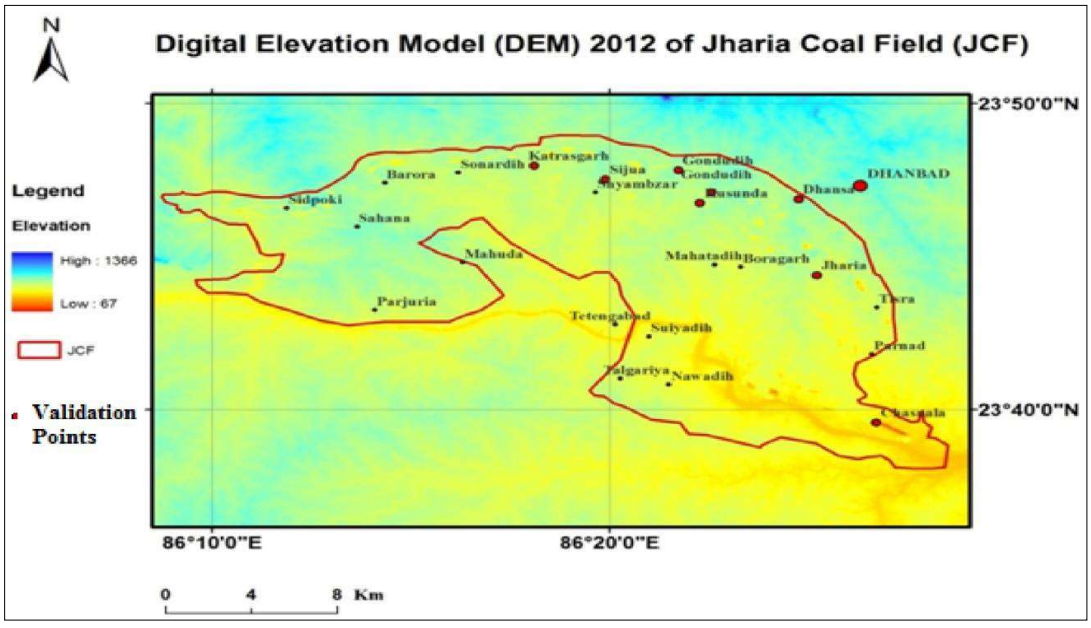

Fig: 70 Validation points with GPS location in field superimposed on DEM of 2012

Table: 17 Results of K – Means

Sl.No	Class	Pixels	Pixels checked in field	accurate pixels	Accuracy	Percentage
1	Class1	44235	200	158	0.79	79
2	Class2	82532	200	143	0.715	71.5
3	Class3	81651	200	165	0.825	82.5
4	Class4	54531	200	156	0.78	78
5	Class5	85942	200	153	0.765	76.5
6	Class6	52792	200	157	0.785	78.5
7	Class7	94951	200	167	0.835	83.5
8	Class8	82542	200	161	0.805	80.5
9	Class9	84714	200	163	0.815	81.5
10	Class10	63687	200	159	0.795	79.5
11	Class11	104059	200	156	0.78	78
12	Class12	95194	200	154	0.77	77
13	Class13	96028	200	157	0.785	78.5
14	Class14	89941	200	158	0.79	79
15	Class15	107920	200	154	0.77	77
16	Class16	71442	200	164	0.82	82
17	Class17	105776	200	173	0.865	86.5
18	Class18	94600	200	164	0.82	82
19	Class19	76283	200	152	0.76	76
20	Class20	64348	200	154	0.77	77
21	Class21	41826	200	152	0.76	76
22	Class22	50338	200	156	0.78	78
23	Class23	83628	200	157	0.785	78.5
24	Class24	105016	200	154	0.77	77
25	Class25	94515	200	154	0.77	77

Table: 18 Results of MLC

Sl.No	Class	Pixels	Pixels checked in field	accurate pixels	Accuracy	Percentage
1	Class1	1129	200	174	0.87	87
2	Class2	98321	200	178	0.89	89
3	Class3	28875	200	182	0.91	91
4	Class4	2520	200	185	0.925	92.5
5	Class5	22527	200	169	0.845	84.5
6	Class6	18938	200	182	0.91	91
7	Class7	75	75	75	1	100
8	Class8	127056	200	177	0.885	88.5
9	Class9	31098	200	168	0.84	84
10	Class10	13545	200	184	0.92	92
11	Class11	28724	200	186	0.93	93
12	Class12	69211	200	176	0.88	88
13	Class13	67003	200	174	0.87	87
14	Class14	12586	200	173	0.865	86.5
15	Class15	44185	200	176	0.88	88
16	Class16	26125	200	183	0.915	91.5
17	Class17	691039	200	176	0.88	88
18	Class18	6078	200	178	0.89	89
19	Class19	154536	200	182	0.91	91
20	Class20	10435	200	186	0.93	93
21	Class21	17521	200	168	0.84	84
22	Class22	8550	200	176	0.88	88
23	Class23	55017	200	174	0.87	87
24	Class24	402112	200	176	0.88	88
25	Class25	71285	200	179	0.895	89.5

Table: 19 Results after applying recode to MLC classified image

Sl. No	Class	Pixels	Pixels checked in field	accurate pixels	Accuracy	Percentage
1	Dense Forest	43106	200	193	0.965	96.5
2	Open Forest	82532	200	186	0.93	93
3	Open forest scrubs	81651	200	198	0.99	99
4	Degrade forest	54531	200	196	0.98	98
5	Artificial Forest	85942	200	197	0.985	98.5
6	Coal Quarry	52792	200	194	0.97	97
7	Advance Quarry Site	94951	200	197	0.985	98.5
8	Mining pit	82542	200	186	0.93	93
9	Stock	84714	200	185	0.925	92.5
10	Dump	63687	200	178	0.89	89
11	Barren OB	104059	200	194	0.97	97
12	Cultivated Land	95194	200	193	0.965	96.5
13	Fallow Land	96028	200	198	0.99	99
14	Waste land	89941	200	193	0.965	96.5
15	Waste land	107920	200	197	0.985	98.5
16	Siltation	71442	200	196	0.98	98
17	Barren Land	148202	200	194	0.97	97
18	Fly ash pond	94600	200	195	0.975	97.5
19	urban	76283	200	196	0.98	98
20	rural	64348	200	195	0.975	97.5
21	Industrial	41826	200	198	0.99	99
22	surface water body	50338	200	194	0.97	97
23	ponds	83628	200	193	0.965	96.5
24	Water logged area	105016	200	191	0.955	95.5
25	CSF	52089	200	194	0.97	97

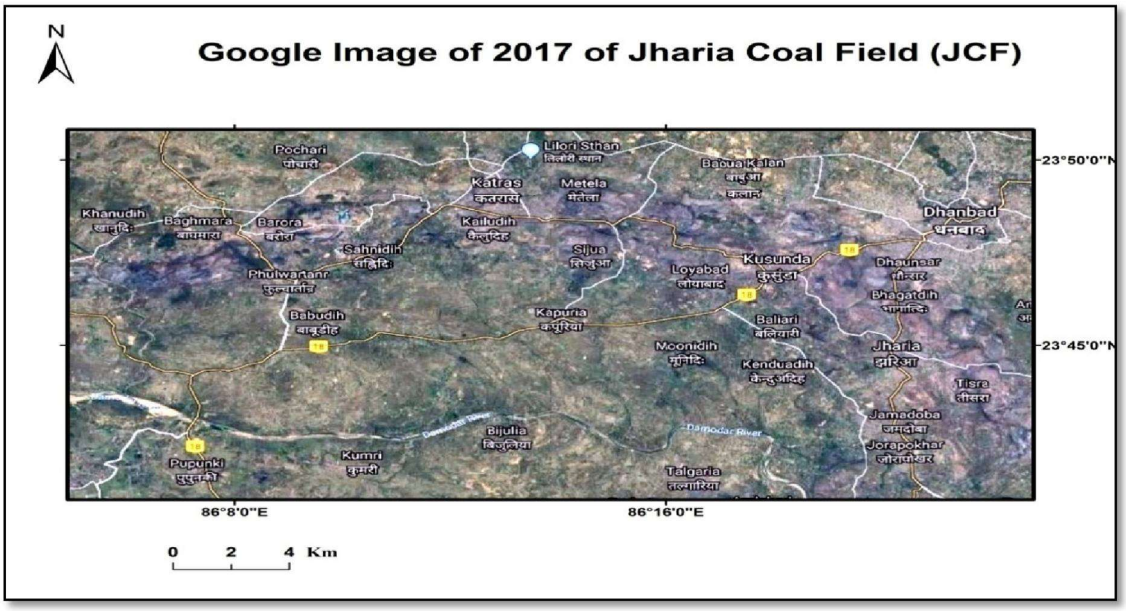

Fig: 71 Validations with Google Image of 2017

The simulated pixels were validated in the field with the Geo tagging with the GPS. The Google Image as used as the latest data for validation of LULC in the field.